sustainability

MDPI

Article

Geothermal Condition Investigation and Resource Potential Evaluation of Shallow Geothermal Energy in the Yinchuan Area, Ningxia, China

Wengang Qu [1,2,3], Chao Yang [4], Hui Qian [1,2,3,*], Panpan Xu [1,2,3], Yanyan Gao [1,2,3], Leiqiang Wei [1,2,3] and Qi Long [1,2,3]

1 School of Water and Environment, Chang'an University, Xi'an 710054, China; wengang_qu@chd.edu.cn (W.Q.); panpanxu@chd.edu.cn (P.X.); gaoyy91@chd.edu.cn (Y.G.); 2021229057@chd.edu.cn (L.W.); 2023029004@chd.edu.cn (Q.L.)
2 Key Laboratory of Subsurface Hydrology and Ecological Effects in Arid Region, Ministry of Education, Chang'an University, Xi'an 710054, China
3 Key Laboratory of Eco-Hydrology and Water Security in Arid and Semi-Arid Regions, Ministry of Water Resources, Chang'an University, Xi'an 710054, China
4 Ningxia Survey and Monitor Institute of Land and Resources, Yinchuan 750004, China; yangchaochd@163.com
* Correspondence: qianhui@chd.edu.cn

Abstract: Shallow geothermal energy (SGE) is a promising green and sustainable energy source, gaining prominence in light of the dual-carbon target. This study investigated the SGE resources in the Yinchuan area. Suitability zones and the potential of SGE resources were determined based on the comprehensive analysis about thermophysical parameters, hydrogeological conditions, and geological environment. Our findings revealed that the effective thermal conductivity in the Yinchuan area surpasses those of other cities, indicating significant potential for SGE. The thermostat layer depth ranges from 40 to 60 m, with a geothermal gradient between 0.81 and 6.19 °C/100 m. Regions with poor adaptability for a borehole heat exchanger (BHE) are mainly distributed in the western and southern parts of the Yinchuan area, whereas moderately and highly adaptable areas are primarily located in the central and eastern areas, respectively. The total geothermal resource of the BHE in the Yinchuan area amounts to 1.07×10^8 GJ/a, generating significant economic benefits of 1.07×10^9 CNY/a and saving 1.09×10^6 t/a of standard coal annually. This initiative leads to significant reductions in CO_2, SO_2, and NOx emissions by 2.61×10^6 t/a, 1.86×10^4 t/a, and 6.57×10^3 t/a, respectively. Additionally, it results in potential savings of 0.309×10^9 CNY/a in environmental treatment costs. The methods and models used in this study have potential for similar geothermal surveys in arid and cold regions. The results also contribute essential insights for policy formulation and sustainable development strategies related to shallow geothermal resources in the Yinchuan area.

Keywords: thermophysical parameters; resource potential; suitability zoning; borehole heat exchanger; shallow geothermal energy

Citation: Qu, W.; Yang, C.; Qian, H.; Xu, P.; Gao, Y.; Wei, L.; Long, Q. Geothermal Condition Investigation and Resource Potential Evaluation of Shallow Geothermal Energy in the Yinchuan Area, Ningxia, China. *Sustainability* **2024**, *16*, 10962. https://doi.org/10.3390/su162410962

Academic Editor: Jin Luo

Received: 29 November 2024
Revised: 10 December 2024
Accepted: 12 December 2024
Published: 13 December 2024

1. Introduction

In recent decades, the rapid expansion of global industry has led to a surge in environmental problems, primarily the emission of greenhouse gases, which has caused an increase in the earth's temperature and exacerbated extreme weather conditions [1–4]. To mitigate greenhouse gas emissions, countries worldwide, including China, have committed to "The Paris Agreement" and devised their emission reduction strategies [5–7]. China, as the most populous developing country, has established ambitious goals, aiming to reach the peak of carbon dioxide emissions by 2030 and achieve carbon neutrality by 2060 [8]. To achieve this objective, a swift transition to renewable energy sources is imperative, replacing fossil fuels.

Geothermal energy, recognized for its rapid regeneration, cleanliness, and environmental preservation qualities, stands out as a viable alternative to conventional fuels [9–12]. Geothermal energy can be classified into shallow (0–200 m), moderate (200–3000 m), and deep (3–10 km) categories based on its development depth [13]. Shallow geothermal energy (SGE) offers the advantages of cost-effectiveness, high efficiency, versatility, and durability compared to moderate and deep geothermal energy [14,15]. Consequently, SGE exhibits significant potential for widespread development and utilization [16–19]. The earliest record of the use of SGE traces back to the 1920s in the United States, gaining substantial traction in the 1980s with the advent of ground-source heat pumps, ushering in a huge market for SGE [20]. SGE has seen global application, spanning regions such as China [21–24], North America [25,26], and Europe [27–30]. Despite its evident advantages and global adoption, the suitability for SGE utilization varies due to geological, hydrogeological, geomorphological, and thermophysical parameter disparities, hence not all places are suitable for the development and use of SGE [31]. Consequently, detailed hydrogeological surveys, ground temperature investigations, thermophysical parameter tests, and resource potential evaluations are essential prerequisites for the effective development and utilization of SGE.

The application of SGE predominantly relies on ground source heat pump technology, extensively used for heating and cooling applications in industrial, commercial, and residential structures [32–35]. Ground source heat pumps are broadly categorized into two types: open-loop systems and closed-loop systems (also known as borehole heat exchanger) [36]. Open-loop systems use groundwater as a heat transfer medium, extracted from the ground and conveyed directly to a nearby heat pump and subsequently reintroduced into the aquifer or in surface waters, or in sewer network [37,38]. However, due to limited recharge efficiency, the pumped groundwater cannot be completely recharged back to the aquifer. Consequently, Open-loop systems would lead to groundwater wastage, making them unsuitable for the areas with scarce groundwater resources and low recharge. In contrast, closed-loop systems use pure water or a water-antifreeze mixture circulating through buried pipes, physically isolated from the rock and groundwater [39,40]. With no direct use of groundwater, closed-loop systems have minimal impact on groundwater and aquifers. Therefore, this study concentrates on suitability zoning and energy potential evaluating specific to the borehole heat exchanger (BHE).

Various methods exist for suitability evaluation, including the analytic hierarchy process (AHP) [41], the G.POT model [42,43], and the TOPSIS model [23,44]. Owing to its comprehensive, simple, and practical nature, and its ability to function with limited quantitative data, the AHP finds widespread application in hydrology [45], ecology [46], environment [47], and energy sectors [48,49], particularly in studies related to SGE [24,50–53]. Consequently, in this study, the AHP is employed for suitability zoning in SGE utilization.

Yinchuan, the capital of Ningxia, is a strategic node city in "The Belt and Road" [54], and an important city in "The Yellow River Basin's Ecological Protection and High-quality Development Plan". Its long and cold winters [55] necessitate significant consumption of urban heating, leading to the emission of greenhouse gas. To mitigate this environmental impact, the shift to renewable energy, specifically SGE, presents a viable solution. However, despite its potential, the high costs associated with preliminary surveys have hindered extensive SGE use in the Yinchuan area. Previous studies have been limited to the main urban areas, neglecting the surrounding districts and counties [56]. A comprehensive survey and research SGE resources in the Yinchuan area are necessary.

This study delves into the hydrogeological conditions and geothermal distribution characteristics of the Yinchuan area, while also conducting thermophysical parameters tests. On this basis, the suitability zoning and SGE resources evaluation are carried out. This study aims to: (1) identify the geothermal, hydrogeological and geological environment in the Yinchuan area; (2) assess the suitability of the BHE in the Yinchuan area; (3) evaluate SGE potential through the heat capacity and heat exchange power (HEP); (4) evaluate the economic and environmental benefits by the development and utilization of the BHE. The research findings can assist decision-makers in formulating scientific policies for the

sustainable utilization of SGE in the Yinchuan area. It also provides references for the investigation and evaluation of SGE in arid and cold regions.

2. Study Area

The Yinchuan area is located in the northern part of the Ningxia Hui Autonomous Region, in the middle of Yinchuan Plain, bordered by the Yellow River to the east and the Helan Mountains to the west. It comprises three districts (Xixia, Jinfeng, and Xingqing) and two counties (Helan and Yongning), covering an area of approximately 2856.19 km^2 and a population of about 2.5 million (Figure 1a) [57].

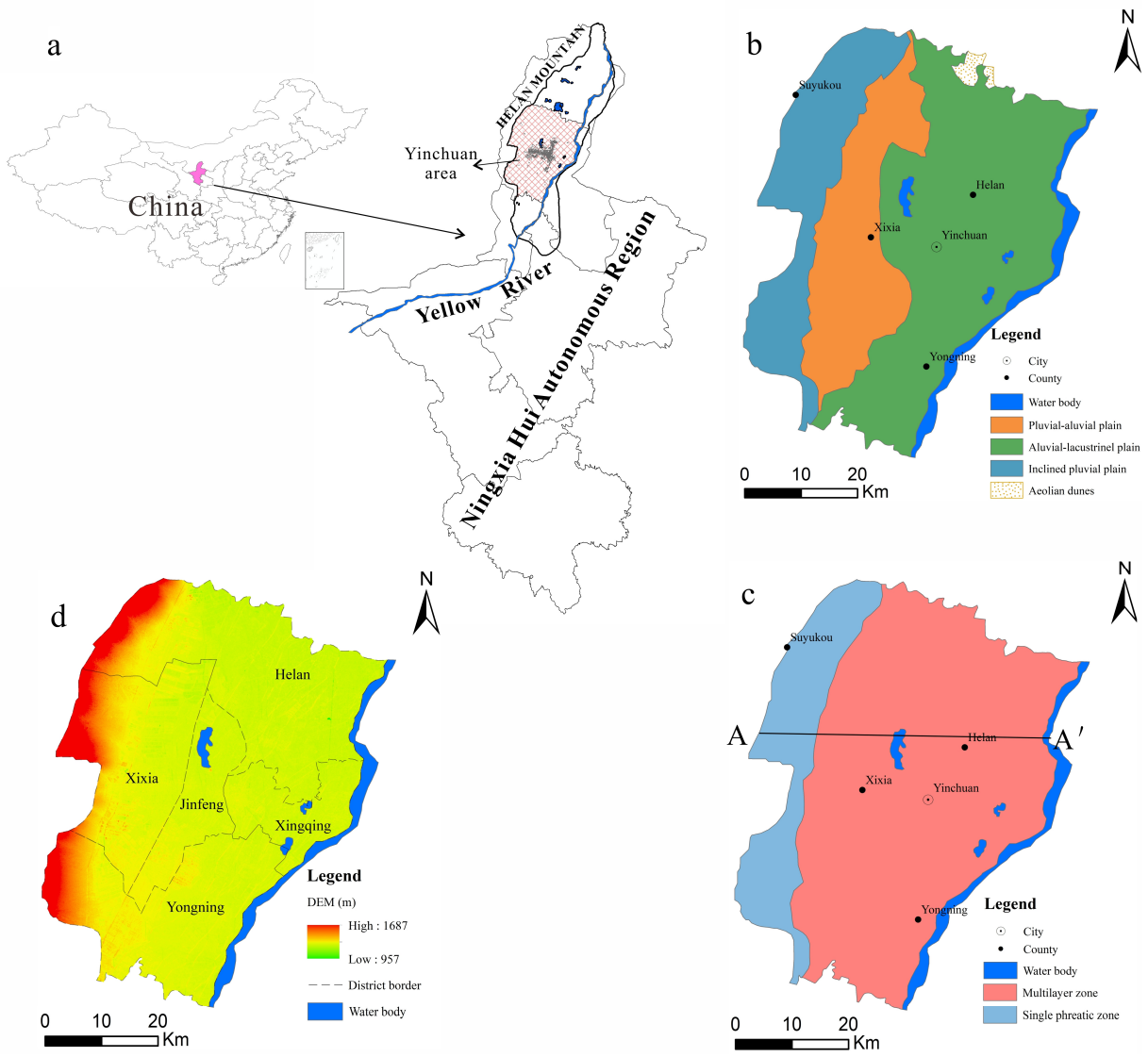

Figure 1. Maps showing the location (**a**), geomorphology (**b**), hydrogeology (**c**), and DEM (**d**) of the study area.

The landforms in the study area pass from inclined pluvial plain in the west to pluvial–alluvial plain in the central region and finally to alluvial–lacustrine plain in the east, with some aeolian sand dunes in the northern part (Figure 1b). The study area exhibits distinct geological features: the western part is characterized by a single lithology composition and is referred to a single phreatic zone. In contrast, the central and eastern areas exhibit complex lithology, forming multi-layered structural zones [58] (Figure 1c). The multi-layered structural zones can further be divided into the phreatic aquifer, the first confined aquifer, the second confined aquifer, and two aquitards [59]. The groundwater hydraulic

gradient gradually decreases from west to east, the groundwater table usually buried beyond 10 m in the inclined alluvial plain and less than 4.6 m in the alluvial lacustrine plain [60]. The DEM of the study area ranged from 957 to 1687 m, as shown in the Figure 1d.

The study area experiences a temperate continental climate characterized by long winters, short summers, low precipitation, and high evaporation rates [61,62]. The annual average temperature, precipitation, and evaporation are 10.36 °C, 183.59 mm, and 1662.33 mm, respectively [63]. The maximum monthly average temperature reaches 29.9 °C, while the minimum drops to −12.8 °C. Precipitation mainly occurs between July and September [64] (shown in Supplemental Materials Figure S1). According to the China Meteorological News report, the average days of winter in Yinchuan city are 171 days from 1988–2010 [65]. The prolonged winter significantly augment the heating requirements in the Yinchuan area.

The Quaternary deposits are widely distributed in the study area. The inclined pluvial plain predominantly consists of gravel and sand. The pluvial–alluvial and alluvial–lacustrine plains predominantly consist of fine sand, sandy clay, and clayey sand interlayers (Figure 2) [66]. Notably, the sand layer in the alluvial–lacustrine plain is relatively thicker than that in the pluvial–alluvial plain [67].

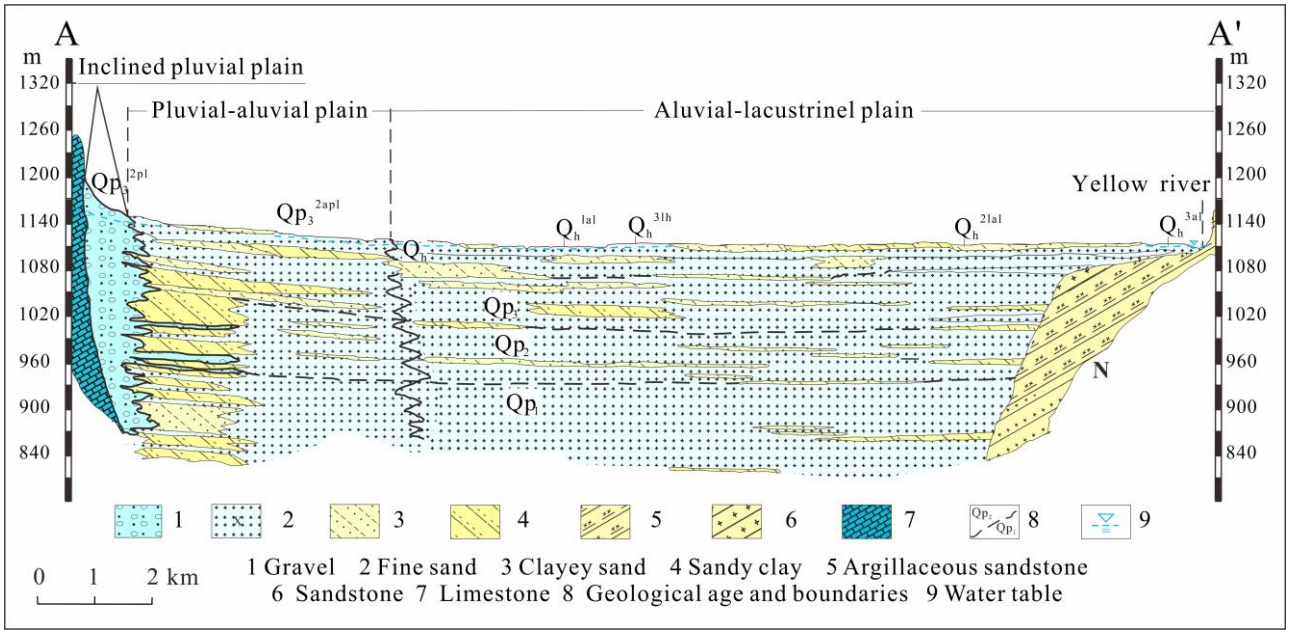

Figure 2. Hydrogeological profile of the study area (**A**,**A′**), modified from [66].

3. Data and Methods

3.1. Data Acquisition

In this study, nine thermal response test holes were drilled to determine the effective thermal conductivity of rocks and soils, with the drilling locations shown in Figure 3a. The heat exchanger used in this study both are double U-pipes. The effective thermal conductivity and heat transfer rate were determined by using the SGE thermal response tester developed by Beijing Huaqing Ronghao New Energy Development Co., Ltd. (Beijing, China). This involved applying constant heating power to the circulating fluid [68], recording inlet and outlet temperatures of the circulated fluid at specified intervals, and calculating the average temperature. The effective thermal conductivity of rock and soil was then determined using the infinite line source theory [69,70] and the curve fitting method.

During this investigation, 19 temperature monitoring wells were set up in the study area, measuring ground temperatures every 10 m within a depth of 200 m, and subsequently calculating the average ground temperature, as shown in Figure 3a.

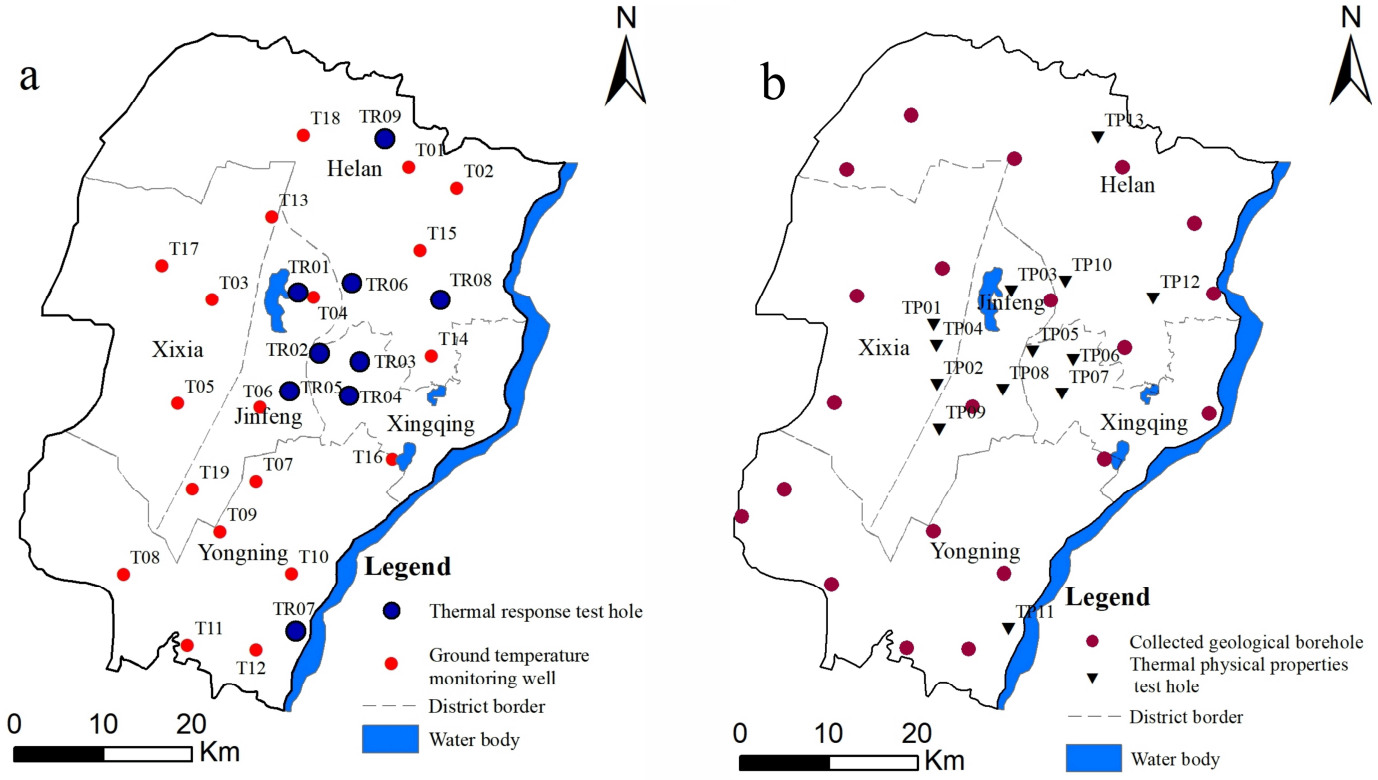

Figure 3. Maps showing the sampling points (**a**) and field test points (**b**) of the study area.

Additionally, 13 thermophysical boreholes were drilled for sample collection and thermophysical property testing in laboratory. A total of 21 geological borehole data were collected to determine the lithological structure of the study area, as shown in Figure 3b. A total of 228 undisturbed samples were collected from the thermophysical boreholes for testing thermophysical parameters such as thermal conductivity and SHC. These samples all were the Quaternary sediments, including 62 silt sand samples, 113 fine sand samples, 44 sandy clay samples, and 9 clay samples.

The plane–source method was used to measure rock and soil thermophysical parameters in the laboratory [71,72]. The primary procedure is outlined as follows: placing the probe between two samples and applying a constant DC. After the probe releases heat, a dynamic temperature field is generated inside the sample, causing a rise in temperature on the probe surface. As a result, the resistance of the probe increases, disturbing the original balanced bridge in the bridge test system. By recording changes in electrical parameters at various intervals during the test, the function representing temperature increase over time was calculated. Fitting this calculated function curve allowed the determination of thermal conductivity and thermal diffusivity for each sample [73].

Geological profile information, including lithology, deposits type, and geological strata, was collected from the geological boreholes. These data served as the basis for analyzing the hydraulic and thermophysical properties of the study area. The thermophysical parameters test data were then assigned to the geological profile boreholes, considering factors such as formation properties and buried depth. The thermophysical parameters were computed as average value weighted by thickness of each rock layer. The distribution of thermophysical parameters across the study area was determined using the Kriging interpolation method.

The hydraulic conductivity of the phreatic aquifer and confined aquifer were collected from the study [74], buried depth of the water table was collected from the 19 temperature monitoring wells, thickness of the aquifer was collected and geomorphology were obtained from the study [75]. The thickness ratio of sand/clay was calculated using geological profile information of boreholes.

3.2. Method

3.2.1. Thermal Response Test Results Calculating Method

According to the line source theory [69,70], the average fluid temperature in the U-tube can be formulated using Equation (1), when the $\alpha_s t/r_b^2 \geq 5$:

$$T_f = \frac{q_l}{4\pi k_s}\left[\ln\left(\frac{4\alpha_s t}{r_b^2}\right) - \gamma\right] + q_l \cdot R_b + T_0 \quad (1)$$

where t is the thermal response test time (s), γ is Euler's constant (0.577216), q_l is the heat transfer rate (W/m), r_b is the radius distance (m), k_s is the effective thermal conductivity [W/(m·°C)], α_s is thermal diffusivity (m^2/s), R_b is borehole thermal resistance [(m·K)/W], and T_0 is the initial soil temperature (°C).

Simplifying Equation (1) through linear regression of temperature and logarithmic time yields Equation (2):

$$T_f = m \cdot \ln(t) + b \quad (2)$$

where m is the slope of the regression line, b is the intercept of the regression line on the Y-axis.

The slope of the average temperature change, calculated by curve fitting, provides the effective thermal conductivity ks as shown in Equation (3):

$$k_s = \frac{q_l}{4\pi m} \quad (3)$$

The heat transfer rate q_l was calculated as follows:

$$q = \frac{\rho_f \cdot V \cdot c_f \left(T_{f,out} - T_{f,in}\right)}{H} \quad (4)$$

where V is fluid flow (m^3/s), $T_{f,out}$ is the outlet fluid temperature (°C), $T_{f,in}$ is the inlet fluid temperature (°C), ρ_f is the fluid density (kg/m^3), c_f is fluid specific heat capacity (SHC) [J/(kg·°C)], q is the heat transfer rate (W/m), and H is the buried depth of the U-pipe (m).

The evaluation framework of this study involved three main tasks: zoning the study area, evaluating resource potential, and assessing economic and environmental benefits as shown in Figure 4. The suitability zoning process comprised three key stages: (1) determining evaluation indicator weights using the analytic hierarchy process (AHP), (2) establishing a scoring system through expert evaluation, and (3) summing the weighted values of each evaluation indicator. The evaluation of resource potential involved computing three primary components, namely, heat capacity, heat exchange power (HEP), and resource potential. Heat capacity calculations were performed for the aeration zone and saturated zones within a depth of 100 m and 200 m using the volume method. Total HEP and resource potential were based on single hole heat exchange power (SHHEP) calculations. Economic benefit evaluation considered available geothermal resources in both summer and winter, while environmental benefit assessment factored in reductions in gas and solid emissions, as well as savings in transportation charges.

3.2.2. Suitability Zoning Method

(1) Determining the weight of evaluation indicators in the zoning system

The AHP model was divided into target layer (A), object layer (B), and indicator layer (C). The target of the AHP model was the suitability zoning of the BHE. The object layer consisted of thermophysical parameters (B1), hydrogeological conditions (B2), geological environmental conditions (B3). Within the AHP, nine evaluation indicators were considered, including thermal conductivity (C1), specific heat capacity (C2), average ground temperature (C3), hydraulic conductivity of phreatic aquifer (C4), hydraulic conductivity of confined aquifer (C5), buried depth of the water table (C6), thickness of the aquifer (C7), geomorphology (C8), thickness ratio of sand/clay (C9).

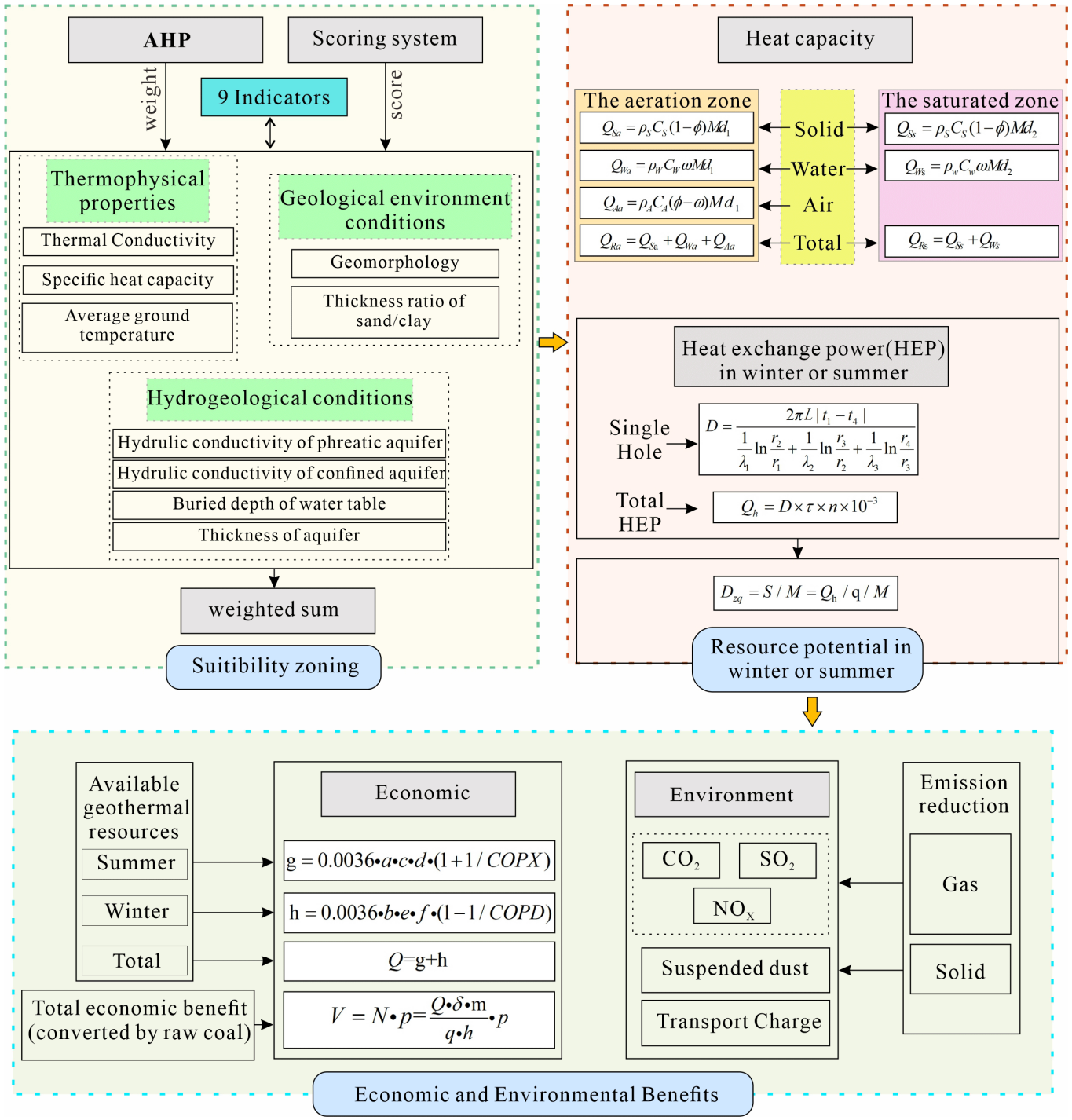

Figure 4. The evaluation framework of the BHE in the Yinchuan area.

Judgment matrices were constructed using the 1–9 scale method [76] as shown in Appendix A Tables A1–A4. Subsequently, the maximum eigen value λ_{max} and corresponding eigenvector ω_i of each matrix were calculated. A ranking consistency test was performed, with, $CR < 0.10$, indicating that the consistency of the judgment matrix was acceptable, otherwise, the judgment matrix should be modified appropriately. The weights of the evaluation system are shown in Appendix A Tables A2–A5.

(2) Establishing the scoring system

Dividing each the BHE evaluation indicators into different sub-areas according to different scores. Scores ranged from 0 to 9, with higher scores indicating greater suitability

for the BHE construction in the sub-area. The lower the score, the less favorable it is for the construction of the BHE in the sub-area. Sub-areas with scores between 0 and 5 were categorized as having poor adaptability, scores between 5 and 7 indicated moderate adaptability, and scores > 7 were the adaptability area [24]. Sub-area scores for the BHE evaluation indicators are shown in Table 1.

Table 1. Evaluation indicators score of the BHE for suitability zoning.

Item	Classification	Score	Item	Classification	Score
Thermal conductivity [w/(m·°C)]	>1.75	9	Thickness of aquifer (m)	>172	9
	1.5–1.75	5		152–172	7
	1.25–1.5	3		132–152	5
	<1.25	1		<132	3
Specific heat capacity [kJ/(kg·°C)]	>1.15	9	Geomorphology	Pluvial–alluvial plain	7
	1.10–1.15	7		Alluvial–lacustrinel plain	9
	1.05–1.10	5		Inclined pluvial plain	3
	1.00–1.05	3		Aeolian dunes	1
	<1	1		Lake	0
Buried depth of water table (m)	<2	5	Thickness ratio of sand/clay	30–100	3
	2–10	9		10–30	9
	10–50	7		5–10	7
	50–100	3		3–5	5
	>100	1		<3	3
Average ground temperature (°C)	>17	9	Hydrulic conductivity of phreatic aquifer (m/d)	5–10	5
	15–17	7		10–20	7
	13–15	5		20–30	9
	<13	3	Hydrulic conductivity of confined aquifer (m/d)	5–10	5
				10–20	7
				single phreatic zone	0

(3) Summing the weights

The study area was divided into a grid of 250 m × 250 m squares, totaling 305 rows, 245 columns, and 74,725 cells. Each evaluation indicator score was assigned to the raster layer using ArcGIS 10.2 software. These scores, combined with indicator weights, were summed to calculate the final suitability zoning score for each cell.

3.2.3. Resource Potential Evaluation Method

In this study, the evaluation standard for SGE resources is based on the "Specification for shallow geothermal energy investigation and evaluation" [77]. The equations used for calculating heat capacity are as follows [24]:

(1) Calculation of heat capacity

In the aeration zone:

$$Q_{Ra} = Q_{Sa} + Q_{Wa} + Q_{Aa} \quad (5)$$

$$Q_{Sa} = \rho_S C_S (1 - \phi) M d_1 \quad (6)$$

$$Q_{Wa} = \rho_W C_W \omega \, M d_1 \quad (7)$$

$$Q_{Aa} = \rho_A C_A (\phi - \omega) M d_1 \quad (8)$$

where Q_{Ra} is the heat capacity (HC) in the aeration zone (kJ/°C), Q_{Sa} is the HC of rock or soil in the aeration zone (kJ/°C), Q_{Wa} is the HC of water in rock or soil (kJ/°C), Q_{Aa} is the HC of the air contained in rock or soil (kJ/°C), ρ_S is the density of rock or soil (kg/m^3), C_S is the SHC of rock or soil [kJ/(kg·°C)], φ is the porosity (or fissure) of soil or rock, M is the calculated area, the value is 2.86 × 10^6 m^2, d_1 is the thickness of aeration zone (m), ρ_w is the density of water, the value is 1000 kg/m^3, C_w is the SHC of water, the value is 4.18 kJ/(kg·°C), ω is the moisture content of rock or soil, ρ_A is the density of air (1.29 kg/m^3), C_A is the SHC of air [1.003 kJ/(kg·°C)].

In the saturated zone:

$$Q_{Rs} = Q_{Ss} + Q_{Ws} \tag{9}$$

$$Q_{Ws} = \rho_w C_w \omega \, M d_2 \tag{10}$$

$$Q_{Ss} = \rho_S C_S (1 - \phi) M d_2 \tag{11}$$

where Q_{Rs} is the HC in the saturated zone (kJ/°C), Q_{Ss} is the HC of rock or soil in the saturated zone (kJ/°C), Q_{Ws} is the HC of water in rock or soil (kJ/°C), d_2 is the thickness of rock or soil from the water table to the calculation lower limit (m).

In this study, d_1 and d_2 were determined based on borehole profile data. Parameters such as density, SHC, porosity, and moisture content were averaged vertically. Kriging interpolation was used to obtain the horizontal distribution grid using ArcGIS 10.2 software. Finally, the HC of the study area was calculated using Equations (5)–(11).

(2) Heat exchange power (HEP)

Based on thermal conductivity, the SHHEP of the 100-m shallow system was calculated using Equation (12) [24]:

$$D = \frac{2\pi L |t_1 - t_4|}{\frac{1}{\lambda_1} \ln \frac{r_2}{r_1} + \frac{1}{\lambda_2} \ln \frac{r_3}{r_2} + \frac{1}{\lambda_3} \ln \frac{r_4}{r_3}} \tag{12}$$

where D is the SHHEP (w), λ_1 is the thermal conductivity of heat exchanger (0.44 W/(m·°C)), λ_2 is the thermal conductivity of backfill materials [W/(m·°C)], λ_3 is the thermal conductivity of the rock or soil around the heat exchange hole [W/(m·°C)], L is the length of borehole heat exchanger (100 m), r_1 is the equivalent inner radius of borehole heat exchanger bundle (0.037 m), r_2 is the equivalent outer radius of borehole heat exchanger bundle (0.04 m), r_3 is the average radius of heat exchange hole (0.1 m), r_4 is the influence radius of heat transfer temperature (5 m), t_1 is the average temperature of circulating fluid in the borehole heat exchanger, according to the technical requirements of the BHE and the results of the thermal response test the value in summer is 31.5 °C and 6.4 °C in winter, and t_4 is the temperature of rock or soil beyond the influence radius (°C). The values of λ_3 and t_4 were obtained from laboratory and field investigations.

The total HEP of the BHE in the moderately adaptable area and the adaptable area was calculated using Equation (13) [24]:

$$Q_h = D \times \tau \times n \times 10^{-3} \tag{13}$$

where Q_h is the total HEP (kW), D is the SHHEP of single hole (W), τ is the land use coefficient of the study area (3.314%), and n is the number of heat transfer holes in the calculated area (the distance between heat exchange holes is 5 m). The total HEP was calculated considering the land use coefficient and without it.

(3) Resource potential of the BHE

The resource potential of the BHE was calculated as follows [77]:

$$D_{zq} = S/M = Q_{\mathrm{h}}/\mathrm{q}/M \tag{14}$$

where D_{zq} is the resource potential of the BHE (m^2/km^2), Q_h is the HEP (kW), M is the total area of moderately adaptable and adaptable areas (km^2), q is heating load in winter or cooling load in summer (W/m^2), 47 W/m^2 for heating load in winter and 69 W/m^2 for cooling load in summer, S is the heating area or cooling area (m^2).

3.2.4. Economic and Environmental Benefits Evaluation

The SGE typically evaluated by drawing analogies with conventional energy (coal burning) to determine the economic benefits. The economic benefits were calculated using Equations (15)–(18) [77]:

$$Q = g + h \tag{15}$$

$$\mathrm{g} = 0.0036 \cdot a \cdot c \cdot d \cdot (1 + 1/COPX) \tag{16}$$

$$\mathrm{h} = 0.0036 \cdot b \cdot e \cdot f \cdot (1 - 1/COPD) \tag{17}$$

$$V = N \cdot p = \frac{Q \cdot \delta \cdot \mathrm{m}}{q \cdot h} \cdot p \tag{18}$$

where Q is the total available geothermal resources (GJ), g is the available geothermal resources in summer (GJ), h is the available geothermal resources in winter (GJ), a is the HEP in summer (kW), b is the HEP in winter (kW), c is heat pump cooling days in summer (90 d), e is heat pump heating days in winter (150 d), d are hours of heat pump operation a day in summer (15 h/d), f are hours of heat pump operation a day in winter (15 h/d), $COPX$ is the heat pump coefficient of performance in summer, the value is 5, $COPD$ is the heat pump coefficient of performance in winter the value is 4, V is the value of heat resources (CNY), N is the quantity of raw coal, t, m is efficient utilization of heat energy (80%), q is the heat produced by burning a kilogram of raw coal (2.09×10^4 kJ), h is boiler thermal efficiency (80%), p is coal price (700 CNY/t), δ is utilization coefficient of SGE (30%).

4. Results and Discussion

4.1. Evaluating Indicators

4.1.1. Geothermal Conditions

The results of the thermal response test are presented in Table 2. The effective thermal conductivity ranges from 1.94 to 2.83 W/(m·°C), and the heat transfer rate ranges from 53.33 to 76.95 W/m. Notably, TR07, located in the southeast of the Yinchuan area, exhibits the highest effective thermal conductivity among the tested sites.

Table 2. Thermal response test results of the Yinchuan area.

Number	U-Type	Depth (m)	Effective Thermal Conductivity [W/(m·°C)]	Heat Transfer Rate (W/m)
TR01	Double	90	2.30	53.33
TR02	Double	125	2.10	56.01
TR03	Double	90	2.32	76.95
TR04	Double	90	2.00	65.11
TR05	Double	90	1.94	74.84
TR06	Double	100	2.27	62.40
TR07	Double	100	2.83	64.80
TR08	Double	100	2.58	64.80
TR09	Double	70	2.05	57.10

To gain a comprehensive perspective on effective thermal conductivity in the Yinchuan area relative to other cities, data were gathered from various regions including the Yangtze River Basin [78], the North China Plain [24,79,80], and Northwest China [81,82], as shown in Table 3. Cities such as Shanghai, Hangzhou, and Nanchang situated in the southern part of China, exhibit effective thermal conductivity ranging from 1.14 to 3.7 W/(m·°C). In contrast, cities in the northern regions, like those in the North China Plain, display

lower values, ranging from 1.32 to 2.71 W/(m·°C). Similarly, cities in northwest China show effective thermal conductivity ranging from 1.09 to 2.32 W/(m·°C). The lithology of the collected cities primarily consists of quaternary deposits. Despite this common geological characteristic, the effective thermal conductivity of cities in northern regions is smaller than that of southern cities due to the higher clay content in the northern areas. This trend is also observed in northwest China. Specifically, when comparing cities like Xi'an, Xianyang, and others with Yan'an and Tongchuan, the latter cities exhibit smaller effective thermal conductivity owing to their elevated clay content. Although the effective thermal conductivity of the Yinchuan area does not match that of southern cities in China, it is relatively larger than that of cities in northern China. The significant difference in effective thermal conductivity indicates that the Yinchuan area possesses the high potential for shallow geothermal energy.

The laboratory measurement results of the different material thermophysical indicators are shown in Table 4. Notably, fine sand displays the highest thermal diffusivity and thermal conductivity, while clay exhibits the lowest values, consistent with previous studies [83]. Two key factors influence these thermophysical parameters: texture and mineral content [84], and grain size of the soil [85]. Fine sand, with its larger grain size and higher quartz mineral content compared to clay, demonstrates significantly higher thermal diffusivity and thermal conductivity.

Table 3. Effective thermal conductivity of main cities in China.

Area	City	Deposits	Effective Thermal Conductivity [W/(m °C)]	Source
Yangtze River Basin	Shanghai	Quaternary deposits, material types consist of clay, silt, find sand and sand.	1.51–2.44	[78]
	Hangzhou	Quaternary deposits, material types consist majorly of clay, silt, find sand and gravel.	1.65–2.66	
	Nanchang	Quaternary deposits, material types consist of clay, silt, fine sand and gravel.	1.14–3.70	
North China Plain	Beijing	Quaternary deposits, material types consist of sand, gravel and clay.	1.97–2.71	[79]
	Tianjin	Quaternary deposits, sand, sandy soil and clay interbed irregularly.	1.55–1.89	
	Zhengzhou	Quaternary deposits, material types consist of clay, silty clay, silt, coarse, medium and fine sand.	1.68–2.07	
	Dezhou	Quaternary deposits, material types consist of silt soil, silty clay, clay, silty sand and fine sand.	1.54–1.89	[80,86]
	Liaocheng		1.32–2.07	
	Linqing		1.74–1.94	
	Linqu		1.53–2.34	[24]
Northwest China	Yan'an, Tongchuan	Quaternary deposits, material types consist of majorly silty clay, silty sand.	0.81–1.34	[81]
	Xi'an, Baoji, Xianyang, Weinan	Quaternary deposits, material types consist of different grain size sand, soil.	1.09–1.83	[82]
	Yinchuan area	Quaternary deposits, material types consist of silty sand, fine sand, sandy clay and clay.	1.94–2.83	this study

A comparison of borehole thermal parameters between this study and other cities is provided in Table 5. Cities in southern China, such as Shanghai, Hangzhou, and Nanchang, exhibit thermal conductivity ranging from 1.03 to 2.77 W/(m·°C), 1.22 to 2.72 W/(m·°C), and 1.44 to 3.63 W/(m·°C), respectively. In contrast, cities in Northern China, including Beijing, Tianjin, and Linqu demonstrate lower thermal conductivity, ranging from 1.47 to 2.02 W/(m·°C), 1.26 to 1.62 W/(m·°C) and 1.25 to 1.9 W/(m·°C), respectively. The findings

emphasize that cities in Southern China generally exhibit higher thermal conductivity compared to those in Northern China.

Table 4. Laboratory test results of thermophysical parameters in the Yinchuan area.

Deposit	Silty Sand	Fine Sand	Sandy Clay	Clay
Num.	62	113	44	9
Moisture content ω (%)	19.492 ± 3.779 *	19.850 ± 3.607	23.323 ± 3.570	23.211 ± 4.738
Porosity n (%)	36.274 ± 3.577	35.740 ± 4.180	39.973 ± 3.874	38.911 ± 4.038
Thermal diffusivity α (mm^2/s)	0.0032 ± 0.0007	0.0034 ± 0.0007	0.0023 ± 0.0006	0.0020 ± 0.0003
Thermal conductivity λ [W/(m·°C)]	1.931 ± 0.276	2.032 ± 0.308	1.452 ± 0.263	1.399 ± 0.206
Specific heat capacity C [kJ/(kg·°C)]	1.084 ± 0.118	1.074 ± 0.119	1.155 ± 0.127	1.234 ± 0.131

*, Mean value ± SD.

Table 5. Thermal parameters collected from other studies.

City	Source	Thermal Conductivity λ [W/(m·°C)]			Specific Heat C [kJ/(kg·°C)]			Thermal Diffusivity α (mm^2/s)		
		Min	Max	Mean	Min	Max	Mean	Min	Max	Mean
Shanghai	[78]	1.03	2.77	1.75	0.6	1.99	1.31	0.33	1.79	0.72
Hangzhou	same as above	1.22	2.72	1.87	0.51	2.33	1.3	0.38	1.33	0.78
Nanchang	same as above	1.44	3.63	1.94	0.59	1.45	0.96	0.5	1.88	0.95
Beijing	[87]	1.47	2.02	-	2.32	3.08	-	0.45	0.84	-
Tianjin	[88]	1.26	1.62	-	1.90	2.20	-	0.44	0.74	-
Linqu	[24]	1.25	1.9	-	0.85	1.24	-	0.42	1.02	-
Yinchuan	this study	1.45	2.17	1.95	0.97	1.20	1.08	0.59	1.09	0.91

In the Yinchuan area, the thermal conductivity ranges from 1.45–2.17 W/(m·°C), with a mean value of 1.95 W/(m·°C). Notably, this value is smaller than the thermal conductivity of the southern China city of Nanchang, as shown in Table 5. This finding aligns with the effective thermal conductivity results, highlighting the high potential of the Yinchuan area for shallow geothermal energy.

The TRT can give the useful information of thermal conductivity about the field location, but the limited time and funds can't conduct intensive thermal response tests in the preliminary shallow geothermal investigation. Laboratory measurements of thermophysical parameters offer a convenient alternative. Moreover, leveraging abundant geological borehole data in the study area allows for a comprehensive characterization of thermophysical parameter distribution across different strata. Consequently, TRT results combined with laboratory-measured thermophysical parameters are employed as key indicators to evaluate the suitability zone of SGE in this study. It is worth noting that thermal response testing is necessary before applying the BHE in the suitable zone, because accurate thermophysical parameters will provide important information for the BHE load design.

As shown in Figure 5a, the average ground temperature in the Yinchuan area ranges from 11.48 °C to 17.18 °C. Higher average ground temperatures are observed in the north-central and southwest regions, reaching a peak of 17.18 °C at T01. T01 is located near a significant concealed fault in Yinchuan [89], suggesting that the high ground temperature might be related to geothermal anomalies caused by the fault. Conversely, lower average ground temperatures characterize the central and southeast regions, with the lowest temperature recorded at 11.48 °C at T12.

Figure 5b illustrates that the depth of the thermostat layer ranges from approximately 40–60 m. Below 60 m, the ground temperature gradually increases. The geothermal

gradient in the study area ranges from 0.81 to 6.19 °C/100 m. T01 displays the highest geothermal gradient, while T12 exhibits the lowest, consistent with the distribution patterns of average ground temperatures. Geothermal gradient anomalies are also related to hidden faults in Yinchuan. Higher formation temperature and larger temperature gradient are advantageous for the heat exchange of the BHE in the winter.

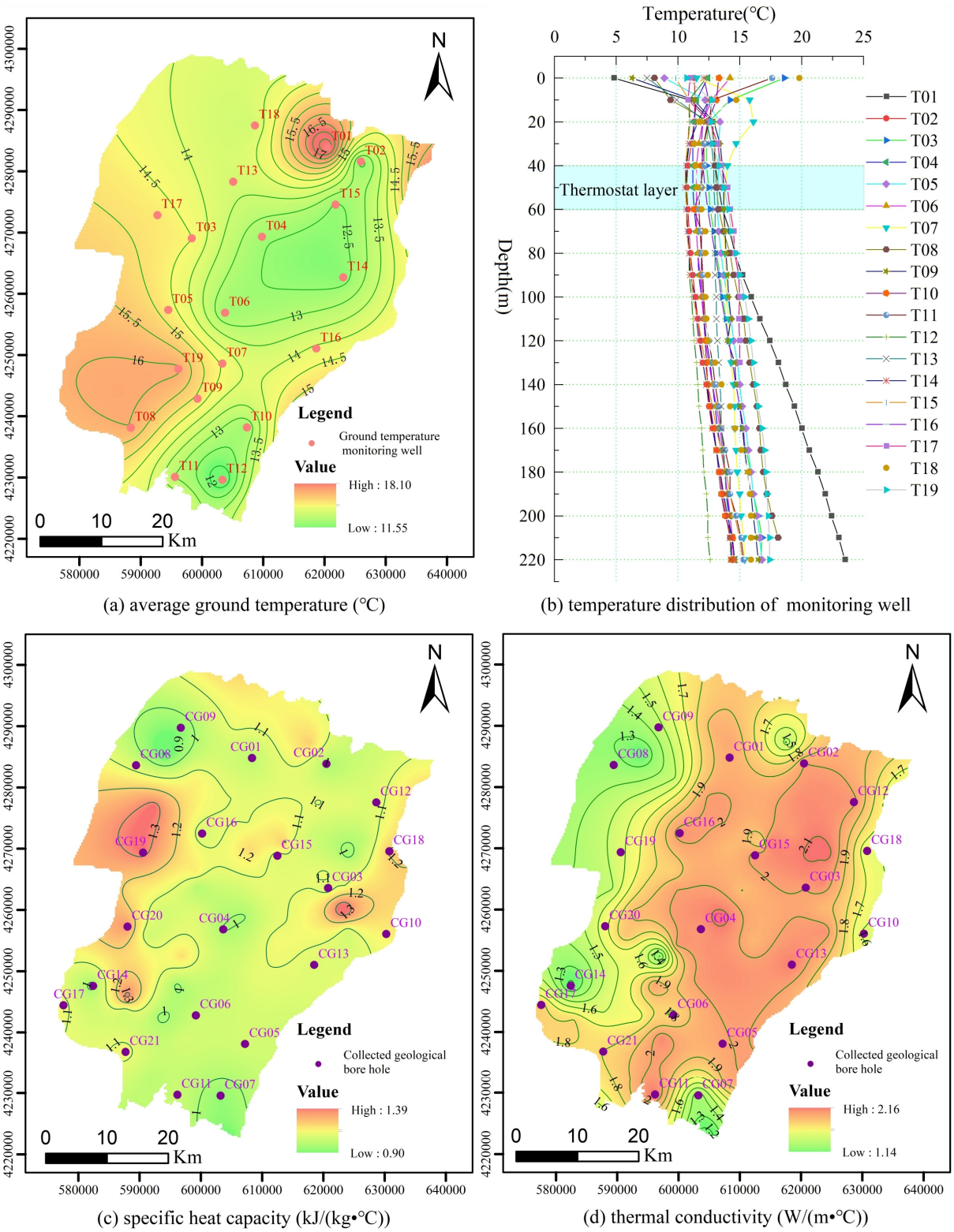

(a) average ground temperature (°C)

(b) temperature distribution of monitoring well

(c) specific heat capacity (kJ/(kg•°C))

(d) thermal conductivity (W/(m•°C))

Figure 5. Geothermal geological conditions in the Yinchuan area.

Upon matching laboratory thermophysical parameters data with borehole profile information, Figure 5c,d illustrate the spatial distribution characteristics of thermophysical parameters of each borehole on the plane. SHC in the Yinchuan area ranges from 0.90 to 1.39 kJ/(kg·°C). Most areas exhibit values below 1.2 kJ/(kg·°C), with only small regions in the west and east exceeding 1.2 kJ/(kg·°C). Thermal conductivity varies between 1.14 and 2.16 kJ/(kg·°C), with the majority of the Yinchuan area exceeding 1.6 kJ/(kg·°C), except for limited areas in the western and southeastern regions, where it falls below 1.6 kJ/(kg·°C).

4.1.2. Hydrogeological Conditions

The hydraulic conductivity of phreatic aquifer ranges from 5 to 30 m/d, as shown in Figure 6a. The hydraulic conductivity of confined aquifer ranges from 5 to 20 m/d, gradually decreases from the center to both sides, as shown in Figure 6b. In Figure 6c, a discernible trend can be observed in the buried depth of the water table, with the western part exhibiting the greatest depth, surpassing 20 m, but the central and eastern parts display comparatively shallower depths, measuring less than 5 m. The distribution characteristic of the aquifer thickness is shown in Figure 6d, the aquifer thickness of most area exceeds 130 m, except the southeast part.

4.1.3. Geological Environment Conditions

The geological environment is characterized by two key indicators: geomorphology and the ratio of sand thickness to clay thickness. The details of geomorphology have been discussed in Section 2 and will not be repeated here. The thickness ratio of sand/clay in the Yinchuan area is shown in Figure 7. Notably, it ranges from 15 to 180. The western part of the study area has the highest value, which gradually decreases from west to east. This variation may be primarily attributed to differences in lithology differences across the study area. Specifically, the western area is characterized by an inclined pluvial plain, predominantly composed of sand and gravel with minimal clay content. In contrast, the central part is a pluvial–alluvial plain consisting of gravel, sand, and clay, with a clay layer that progressively increases. Finally, the eastern part is the alluvial–lacustrine plain, where the lithology is primarily composed of interbedded sand and clay, and the clay layer thickness further increases.

4.2. Suitability Zoning of the BHE

The suitability zoning serve provide a basis for further evaluation and exploitation of SGE resources in the study area. Once the weight matrix, the score system, and weighted summing are constructed, the suitability zoning map of the 200-m BHE in the Yinchuan area is obtained as shown in Figure 8.

This study demonstrates that the Yinchuan area is partitioned into three distinct zones based on the BHE adaptability, namely the adaptability area, moderate adaptability area, and poor adaptability area. The poor adaptability area covers about 499.11 km^2, accounting for 17.47% of the study area, and it is mainly distributed in the western and southern parts of the study area. The features of evaluation indicators related to the low suitability zone in the western study area are outlined as follows: the hydraulic conductivity of phreatic aquifer predominantly 20–30 m/d, while the lithology of the formation primarily consists of sand gravel. Moreover, the thermal conductivity is below 1.5 W/(m °C), and the burial depth of the phreatic water exceeds 50 m. Although the hydraulic conductivity of phreatic aquifer is excellent, the formation lithology, the thermal conductivity and the water table burial depth conditions are not suitable for designing and constructing the BHE [31]. Hence, the western study area was designated as a region with low suitability. Moving on to the southern study area, it is characterized by formations consisting of alternating layers of sand and clay, with phreatic water situated at depths ranging from 2 to 10 m. The SHC is measured to be less than 1.0 kJ/(kg °C), while the average ground temperature remains below 13 °C. Additionally, the thermal conductivity is found to be less than 1.5 W/(m °C). The geological type and the buried depth of phreatic water conditions

in the southern study area are well, but the SHC, the average ground temperature and the thermal conductivity conditions are bad, which leads to the southern study area was classified as poor adaptability area.

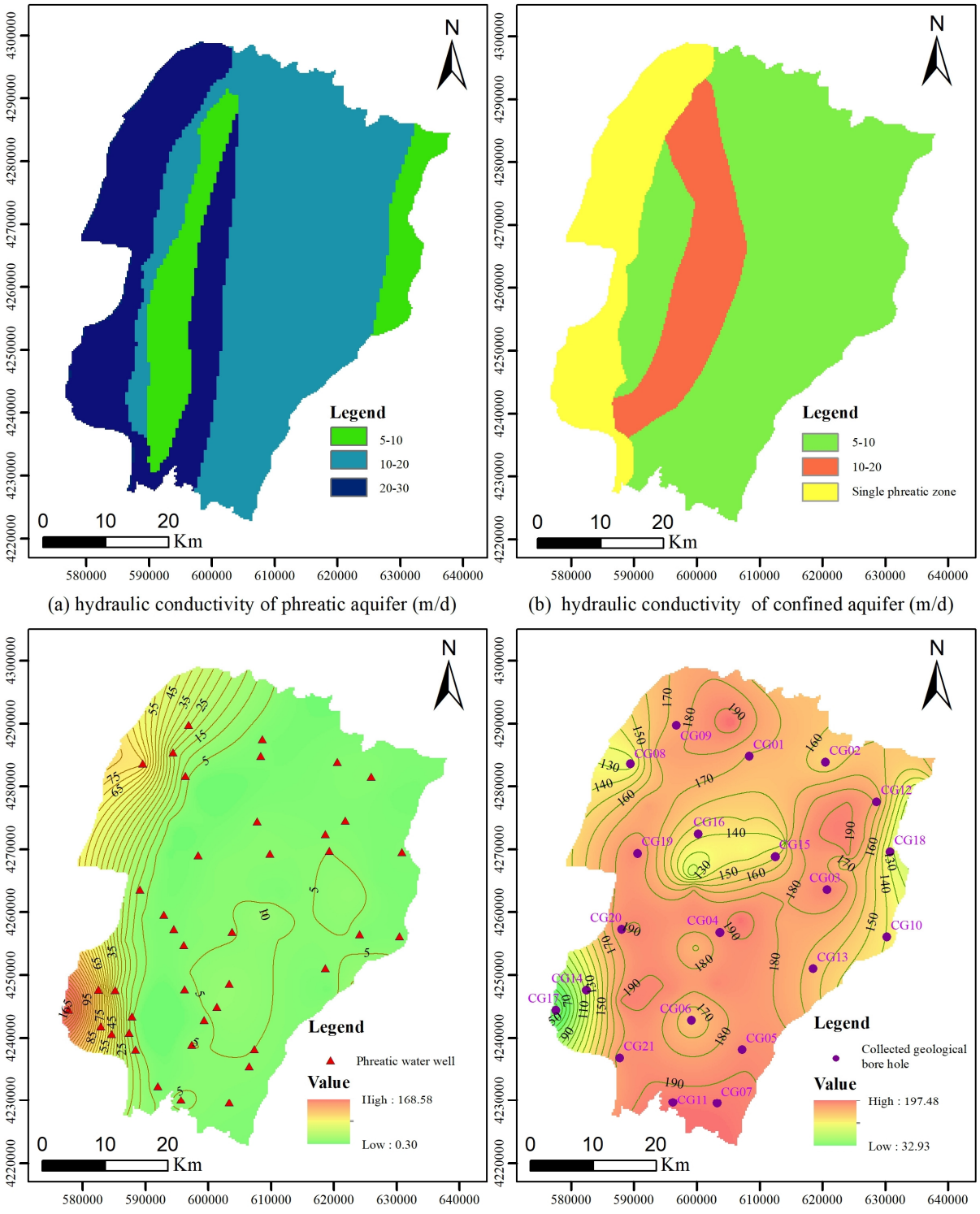

Figure 6. The hydrogeological conditions in the Yinchuan area.

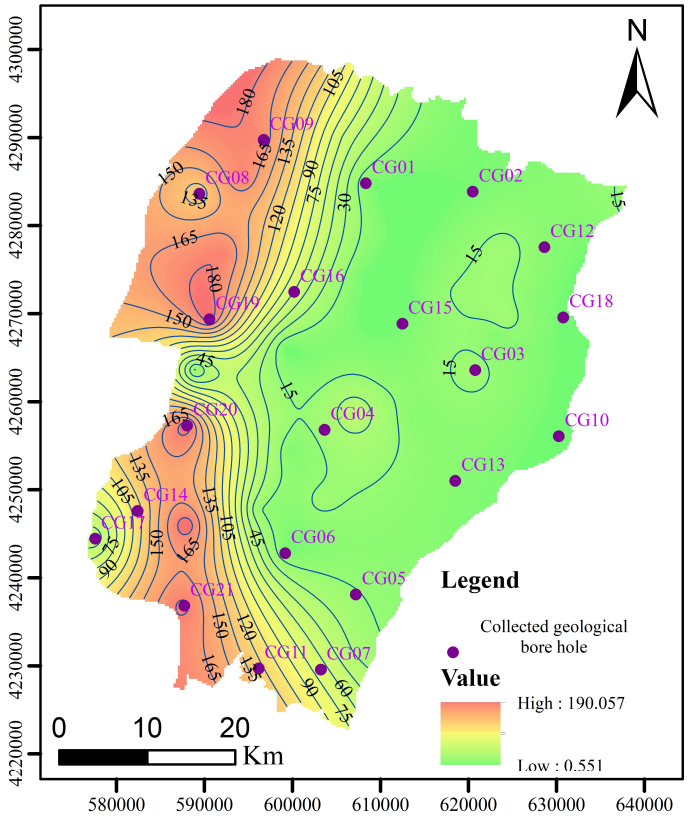

Figure 7. The thickness ratio of sand/clay in the Yinchuan area.

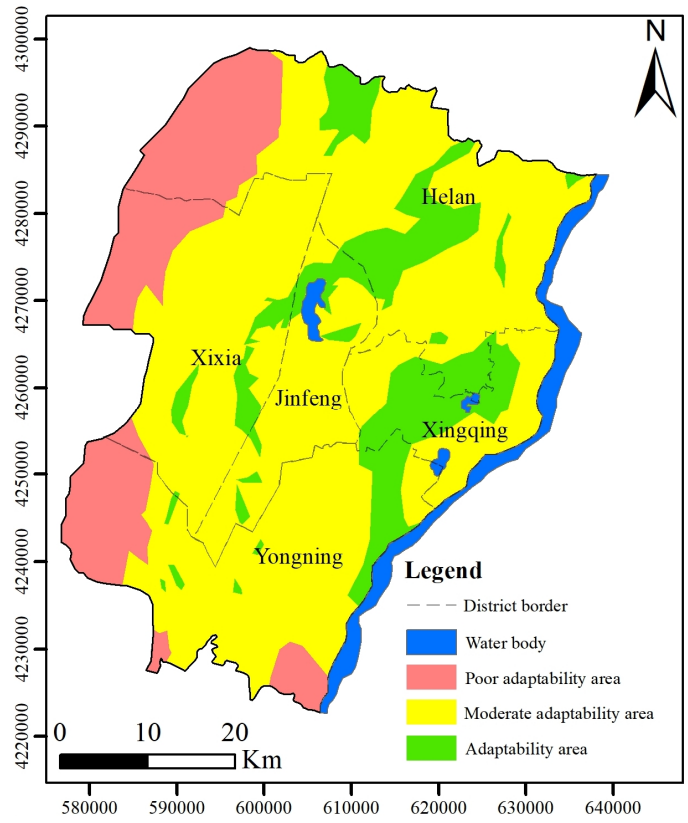

Figure 8. Suitability zones of the BHE in the Yinchuan area.

The adaptability area covers about 438.00 km^2, constituting 15.34% of the total study area, while the moderate adaptability area covers approximately 1919.08 km^2, accounting for 67.19% of the study area. These two areas collectively constitute about 82.53% of the study area and are primarily situated in the central and eastern parts of the study area. The evaluation indicators comprise several characteristics, including the sand–clay thickness ratio, which generally remains below 30. Moreover, the average ground temperature predominantly below 15 °C, with the SHC exceeding 1.0 kJ/(kg·°C) and the thermal conductivity surpassing 1.75 W/(m·°C). The aquifer thickness is larger than 132 m, while the depth of the phreatic water is less than 50 m and the hydraulic conductivity of phreatic aquifer mainly ranges from 5–20 m/d.

Unlike the region with poor suitability, both the moderately suitable and highly suitable areas showed notable impacts from SHC, thermal conductivity, aquifer thickness, depth of phreatic water table, as well as hydraulic conductivity of confined and phreatic aquifer. The evaluation indicator characteristics also are compared in the areas of moderate adaptability and adaptability, the distribution characteristics of SHC align with those of the adaptability area, suggesting the significant of the SHC in the adaptability area. The above description demonstrates that suitability zoning is a systematic work, in which different indicators have different contribution, thus the influence of various indicators on the BHE should be fully considered in suitable zoning to avoid improper zoning results [90].

4.3. Evaluation of the Resource Potential of the BHE

4.3.1. Heat Capacity (HC)

To calculate the HC, the study area was divided into three sub-regions based on landforms, namely the inclined pluvial plain (I), pluvial–alluvial plain (II), and alluvial–lacustrine plain (III), as shown in Figure 1b. Next, the volume method was employed to calculate the heat capacity of the aeration and saturated zones within the depth of 100 m and 200 m and the results are presented in Table 6. The HC in the Yinchuan area within a depth of 100 m is 1.09 × 10^{15} kJ/°C, with a corresponding HC per unit area of 3.82 × 10^{11} kJ/°C/km^2. The HC per unit area of sub-region I is the highest, 5.07 × 10^{11} kJ/°C/km^2, while sub-regions II and III are equivalent, 3.47 × 10^{11} kJ/°C/km^2. The HC within a depth of 200 m is 1.94 × 10^{15} kJ/°C, with a HC per unit area of 6.79 × 10^{11} kJ/°C/km^2. The HC per unit area is highest in sub-region I, followed by sub-regions II and III. Considering the thermophysical indicators and hydrogeological profile, it is evident that sub-region I is primarily composed of sand and gravel, exhibiting high moisture content, porosity, and specific heat capacity, so the HC per unit area is large. In sub-region II and sub-region III, the lithology of the formation both consists with sand and clay layers, with similar thermophysical indicators and negligible disparity in water table burial depth, resulting in a similar amount HC per unit area. The HC per unit area within a depth of 200 m in Yinchuan urban is 4.43 × 10^{11} kJ/°C/km^2 [56].

Table 6. Calculation results of heat capacity in the Yinchuan area.

Sub-Region		I	II	III	Total
Area (km^2)		629.93	682.19	1544.07	2856.19
Aeration zone (kJ/°C)	Q_W	4.56 × 10^{13}	4.32 × 10^{12}	7.78 × 10^{12}	5.77 × 10^{13}
	Q_S	5.26 × 10^{13}	5.50 × 10^{12}	1.03 × 10^{13}	6.84 × 10^{13}
	Q_A	6.06 × 10^{9}	6.48 × 10^{8}	1.30 × 10^{9}	8.00 × 10^{9}
Saturated zone within 100 m (kJ/°C)	Q_W	5.84 × 10^{13}	9.99 × 10^{13}	2.23 × 10^{14}	3.81 × 10^{14}
	Q_S	6.44 × 10^{13}	1.17 × 10^{14}	2.77 × 10^{14}	4.58 × 10^{14}
	Q_R	3.19 × 10^{14}	2.37 × 10^{14}	5.36 × 10^{14}	1.09 × 10^{15}
Heat capacity per unit area within 100 m (kJ/°C/km^2)		5.07 × 10^{11}	3.47 × 10^{11}	3.47 × 10^{11}	3.82 × 10^{11}

Table 6. *Cont.*

Sub-Region		I	II	III	Total
Saturated zone within 200 m (kJ/°C)	Q_W	1.64×10^{14}	2.09×10^{14}	4.53×10^{14}	8.26×10^{14}
	Q_S	1.79×10^{14}	2.46×10^{14}	5.63×10^{14}	9.88×10^{14}
	Q_R	4.41×10^{14}	4.65×10^{14}	1.03×10^{15}	1.94×10^{15}
Heat capacity per unit area within 200 m (kJ/°C/km^2)		7.01×10^{11}	6.81×10^{11}	6.70×10^{11}	6.79×10^{11}

In terms of the HC per unit area within a depth of 200 m in other provincial capitals of China [91], the Yinchuan area is ranked fifth, behind Beijing, Nanjing, Fuzhou, and Xi'an. Moreover, the HC per unit area within a depth of 200 m in the Yinchuan area surpasses the average value (5.14×10^{11} kJ/°C/km^2) of provincial capitals of China (Figure 9). Hence, the SGE resources in the Yinchuan area are important and have the potential to provide a large amount of clean energy.

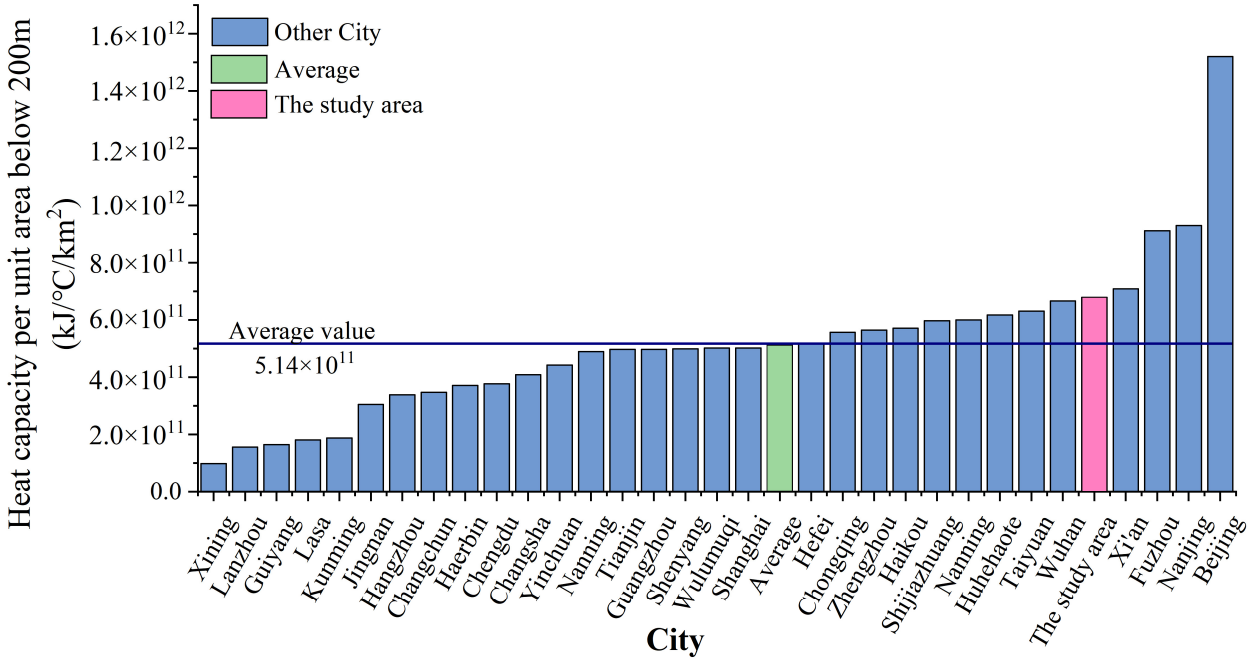

Figure 9. Heat capacity per unit area within a depth of 200 m in China's provincial capitals (data collected from [91]).

4.3.2. Heat Exchange Power (HEP)

Given that the poor adaptability area is not suitable for the application of the BHE, it was not considered when calculating the HEP and the resource potential. The moderate adaptability area and the adaptability area were subdivided into three sub-regions to accurately calculate HEP based on landform characteristics (inclined pluvial plain, pluvial–alluvial plain and alluvial–lacustrine plain), as illustrated in Figure 10. These sub-regions encompass an area of 173.09 km^2, 674.40 km^2, and 1509.59 km^2, respectively. HEP was calculated for both winter and summer, with and without considering the land use coefficient. The results are presented in Figure 11. Considering the land use coefficient, the winter HEP in the Yinchuan area was 5.451×10^6 kW, while in the summer it was 1.265×10^7 kW, which yielded a cumulative HEP of 1.811×10^7 kW. Conversely, in the absence of consideration for the land use coefficient, the winter HEP in the Yinchuan area was estimated to be 1.645×10^8 kW, with the summer HEP reaching 3.819×10^8 kW, resulting in a total HEP of 5.463×10^8 kW. The temperature difference between the borehole heat exchanger circulating liquid and the formation in summer exceeds that of winter, leading to a higher

ability of use formation energy in summer than in winter, and the HEP in summer is higher compared with that in winter [92].

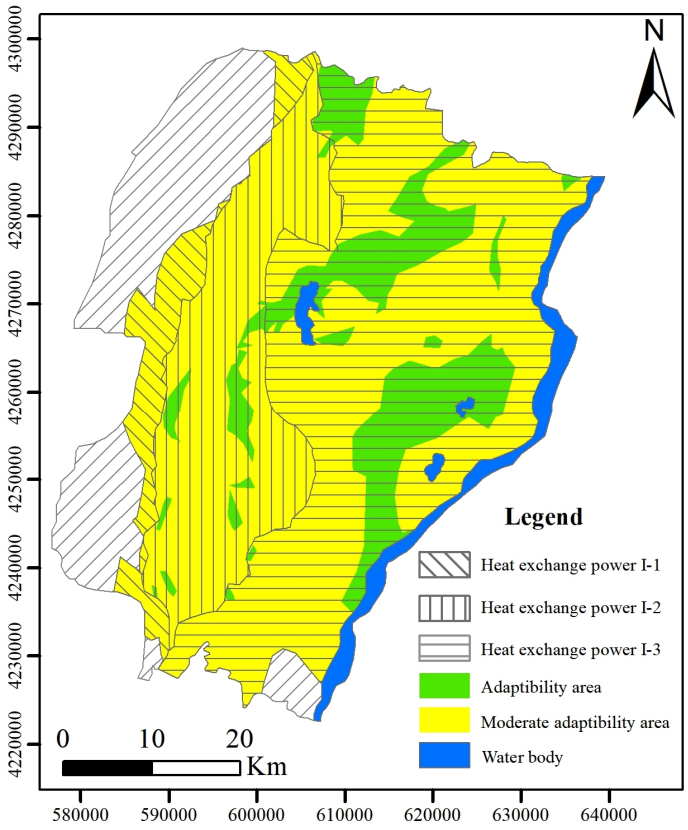

Figure 10. Calculation sub-regions of heat exchange power.

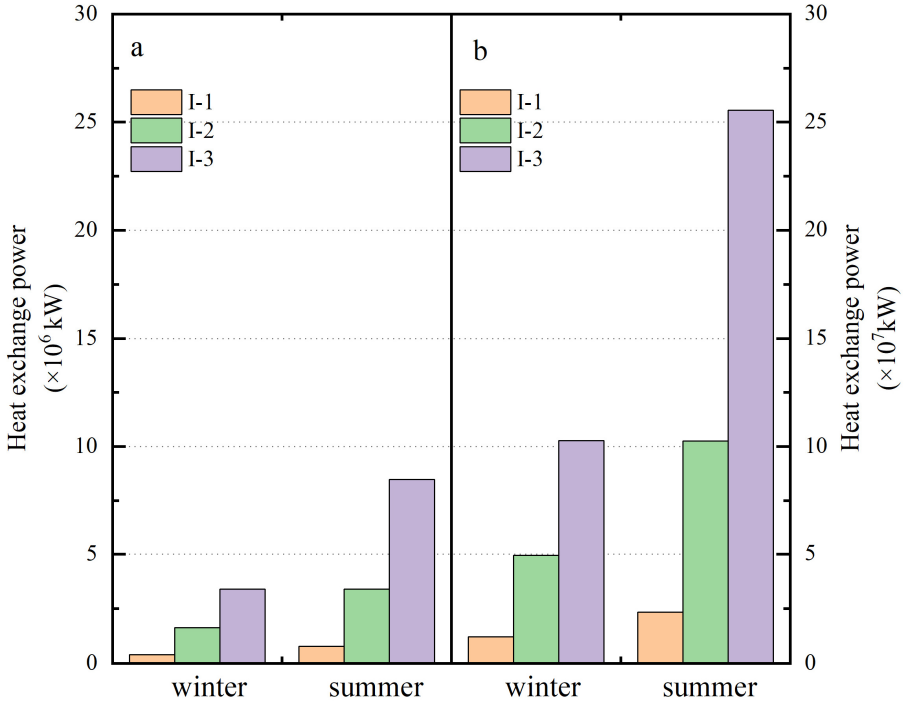

Figure 11. Calculation results of heat exchange power zones of the BHE (**a**) consider the land use coefficient, (**b**) do not consider the land use coefficient.

The distribution of SHHEP in the Yinchuan area was shown in Figure 12. In winter, the SHHEP is between 1052.12 W and 2829.28 W. The highest value was recorded in the Helan county located in the northern part of the Yinchuan area, and the lowest value was obtained in Yongning county situated in the southeast part of the Yinchuan area. In summer, the SHHEP ranges from 2825.25 W to 4879.86 W. It should be mentioned that for most of the Yinchuan area, the SHHEP in summer is relatively high, with the exception of the Xixia district and northern Helan county, where the SHHEP is lower.

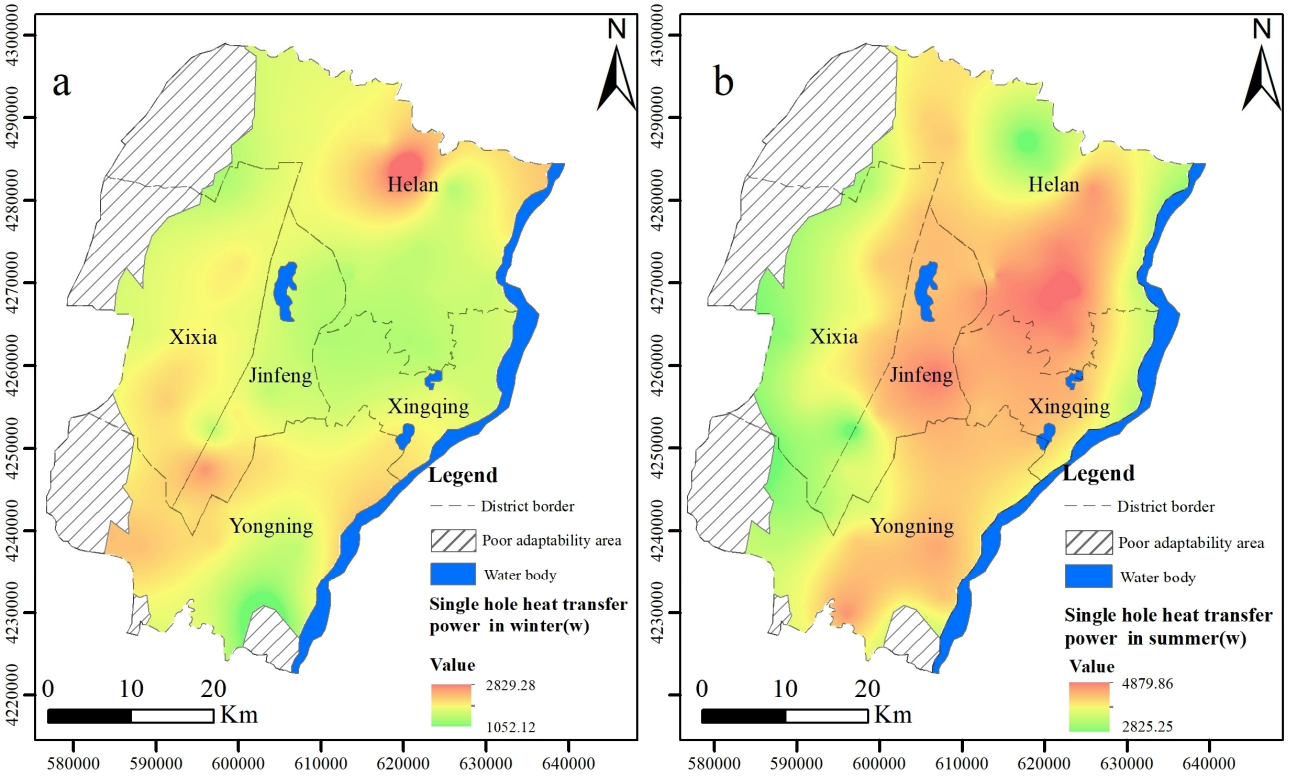

Figure 12. Single hole heat exchange power of the Yinchuan area in winter (**a**) and in summer (**b**).

Analyzing the distribution of SHHEP in winter and the distribution of average ground temperature, results showed that the high value of SHHEP in winter was consistent with the high value of average ground temperature. This highlights the direct impact of the average ground temperature on the SHHEP in winter. Specifically, a higher average ground temperature increases the HEP in winter. It should be noted that the BHE system extracts heat from the formation for heating purposes in winter and inputs heat to the formation for cooling in summer. Therefore, a lower average ground temperature is conducive to heat dissipation in summer. Hence, the distribution law for SHHEP in Yinchuan has an inverse relationship between winter and summer [93].

4.3.3. Resource Potential of the BHE

The results of the resource potential evaluation of the BHE shown in Figure 13 demonstrate that the total heating area of the BHE in the Yinchuan area in winter is 1.16×10^8 m^2, with a corresponding resource potential of 4.92×10^4 m^2/km^2. In contrast, the cooling area during summer is 1.83×10^8 m^2, with a resource potential of 7.78×10^4 m^2/km^2, which exceeds that in winter. The winter potential of sub-region is ranked as I-2, I-1, and I-3, whereas the summer potential of sub-region is ranked as I-3, I-2, and I-1. This study demonstrates that the sub-region rank of SHHEP in winter aligns with the rank of winter potential, whereas the sub-region rank of SHHEP in summer aligns with the rank of summer resource potential. Thus, the quantity of SHHEP is the primary determinant of resource potential.

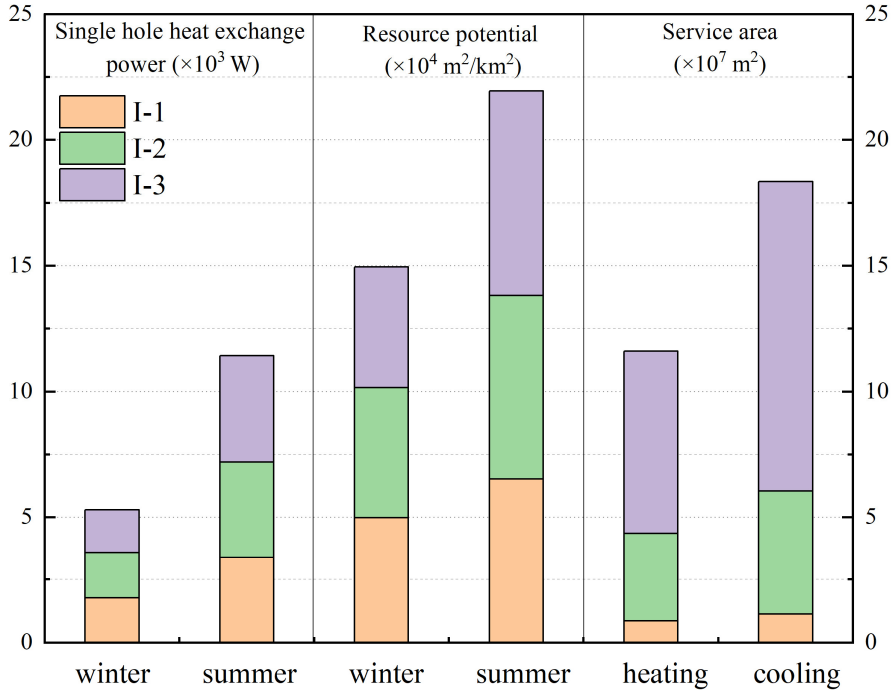

Figure 13. The resource potential evaluation results of the BHE in Yinchuan area.

4.4. Evaluation of Economic and Environmental Benefits

Based on the "General rules for calculation of the comprehensive energy consumption" [94], the conversion coefficient between standard coal and raw coal is set to 0.7143, and the saved standard coal is calculated. The environmental benefits from the emission reduction of the BHE development and utilization in the Yinchuan area was calculated using the "Specification for estimation and evaluation of geothermal resources" (DZ/T 0331-2020) [95] and the emission reduction coefficient and treatment cost per kilogram of standard coal are presented in Table 7.

Table 7. Emission reduction coefficient and treatment cost per kilogram of standard coal.

Emission Reduction Substances	CO_2	SO_2	NOx	Suspended Dust	Ash
Emission reduction coefficient	2.386	1.7%	0.6%	0.8%	10%
Treatment cost (CNY/kg)	0.1	1.1	2.4	0.8	0.04

Figure 14 indicates the calculation results of the available geothermal resources, economic and environmental benefits of the BHE development in the Yinchuan area. Considering the land use coefficient, the annual total usable capacity of the BHE in the Yinchuan area is 1.07×10^8 GJ, and the economic benefits is 1.07×10^9 CNY. The amount of raw coal saved is 1.53×10^6 t, which is comparable to 1.09×10^6 t standard coal. The development and utilization of SGE not only brings about economic benefits, but also reduces the emission of polluting gases. The main air pollutants in Yinchuan are SO_2 and NO_X [96]. Collectively, these results indicate that the SGE can reduce emission of 6.57×10^3 t NO_X, 1.86×10^4 t SO_2, 2.61×10^6 t CO_2 and save 3.09×10^8 CNY in environmental treatment cost per year. The Yinchuan area has great shallow geothermal resource potential. Harnessing SGE has significant economic and environment benefits. Hence, policymakers are encouraged to formulate robust policies for the vigorous development of SGE to propel the region towards green, low-carbon, and sustainable growth, aligning with China's dual-carbon target.

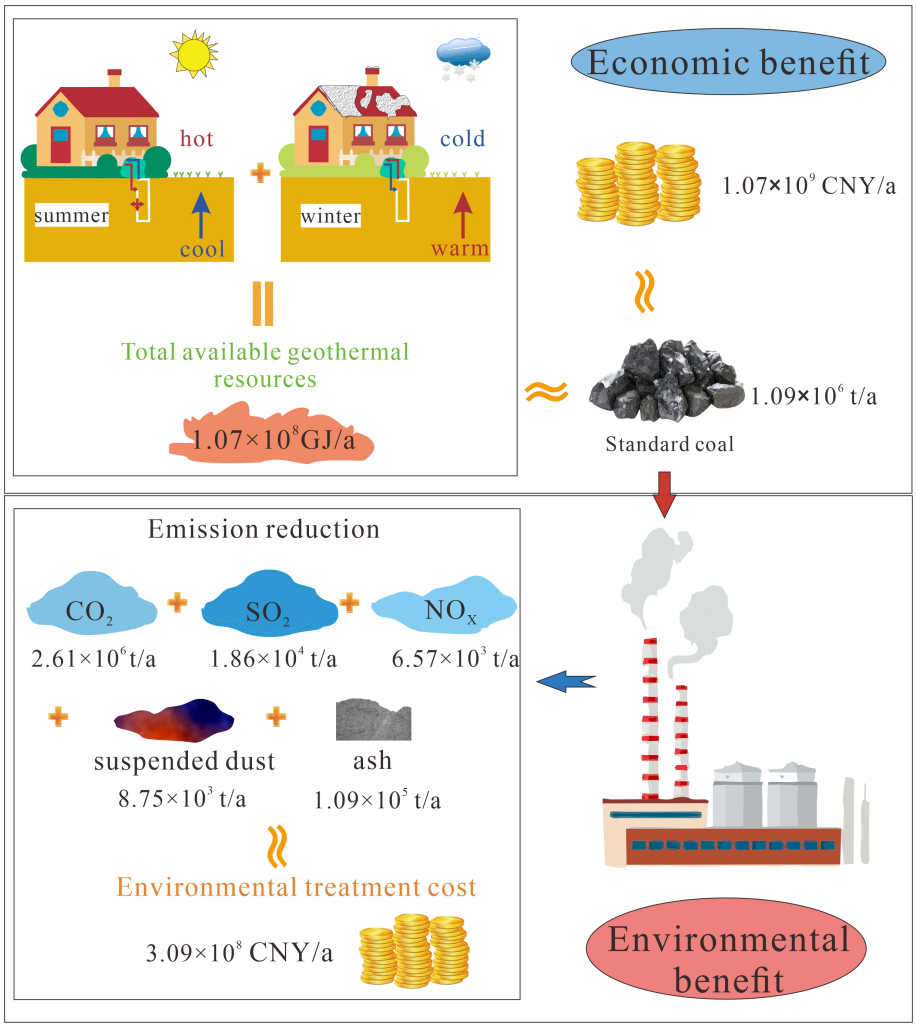

Figure 14. Economic and environmental benefits of the BHE in the Yinchuan area.

5. Conclusions

This paper provided a comprehensive analysis of the thermophysical parameters and hydrogeological conditions in the Yinchuan area. Suitability zones for the BHE were delineated and the resource potential was evaluated accordingly. Additionally, an economic and environmental analysis was conducted. The results and conclusions are outlined below.

The thermal response test results and thermal parameters test indicate that the effective thermal conductivity and thermal conductivity of the Yinchuan area is relatively larger compared with that of north cities of China, suggesting that the Yinchuan area has a high potential for SGE. The thermostat layer depth is about 40–60 m while the geothermal gradient ranges from 0.81 to 6.19 °C/100 m. There are three types of suitability zones for the BHE in the Yinchuan area. Notably, the poor adaptability area is mainly distributed in the western and southern parts of the study area, the moderate adaptability area and adaptability area are primarily situated in the central and eastern parts. The lithology of the formation, thermal conductivity, and depth of the water table burial played a significant role in determining the suitability of certain areas. Additionally, the areas classified as moderately suitable and highly suitable were notably affected by factors such as SHC, thermal conductivity, thickness of the aquifer, depth of phreatic water, confined aquifer hydraulic conductivity, and phreatic aquifer hydraulic conductivity. The BHE not only has great resource potential, but also has significant economic and environmental benefits in the Yinchuan area. When the land use coefficient is taken into consideration, the HEP is 1.81 $\times$ 10^7 kW. The BHE resource potential is 4.92 $\times$ 10^4 m^2/km^2 in winter

and 7.78×10^4 m^2/km^2 in summer. The total available geothermal resource of the BHE is 1.07×10^8 GJ/a, and the economic benefit is 1.07 billion CNY/a. Meanwhile, it can reduce emission of 2.61×10^6 t CO_2, 1.86×10^4 t SO_2, and 6.57×10^3 t NOx and save up to 0.309 billion CNY in environmental treatment cost annually.

The model employed in this study presents valuable insights for evaluating the shallow geothermal energy in arid, cold, or similarly conditioned regions. The evaluation outcomes indicate that the Yinchuan area possesses substantial potential of shallow geothermal energy, and the applying of the BHE will offer significant economic and environmental advantages. We recommend that decision makers to accelerate the development of SGE, devising scientifically sound and standardized development plans, and harness the SGE to expedite the achievement of the dual-carbon target in China. Although the AHP method is applied widely in suitability zoning, the evaluators need to fully understand the basic conditions of the study area, and the impact of subjective judgments on the results should not be ignored. In follow-up research, a comprehensive evaluation framework should be proposed, which considers both subjectivity and objectivity, to obtain more reasonable results.

Supplementary Materials: The following supporting information can be downloaded at: https://www.mdpi.com/article/10.3390/su162410962/s1, Figure S1: Monthly average precipitation and temperature of the study area.

Author Contributions: W.Q., H.Q. and C.Y. designed the study; W.Q. wrote the main manuscript text; L.W. and Q.L. conducted data analysis; H.Q., P.X. and Y.G. reviewed and edited the manuscript text. All authors reviewed the manuscript. All authors have read and agreed to the published version of the manuscript.

Funding: This study was financially supported by the National Natural Science Foundation of China (Grant No. 41931285 and 41790441), the Fundamental Research Funds for the Central Universities, CHD (300102294905), and the Natural Science Foundation of Ningxia (2022AAC03699).

Institutional Review Board Statement: Not applicable.

Informed Consent Statement: Not applicable.

Data Availability Statement: Data will be made available on request.

Acknowledgments: This study was supported by the Ningxia Mining Geological Environment Monitoring and Ecological Restoration Innovation Team. The 'Home for Researchers' (https://www.home-for-researchers.com, accessed on 9 November 2023) polished the original manuscript. We are grateful to the anonymous reviewers and the editors for their valuable comments, which have helped improve the quality of the original manuscript.

Conflicts of Interest: The authors declare no conflicts of interest.

Appendix A

The judgement matrices of the AHP and the calculated results of weights are as follows:

Table A1. A-B Judgment matrix and weight.

A	B1	B2	B3	ω_i
B1	1.00	2.00	3.00	0.540
B2	0.50	1.00	2.00	0.297
B3	0.33	0.50	1.00	0.163
CR		0.007 < 0.1		

Notes: The target layer (A) is the suitability zoning of the BHE. The object layer (B) consisted of thermophysical indicators (B1), hydrogeological conditions (B2), and geological environmental conditions (B3). *CR* is the consistency ratio of the judgment matrix.

Table A2. B1-C Judgment matrix and weight.

B1	C1	C2	C3	ω_i
C1	1.00	1.00	2.00	0.4
C2	1.00	1.00	2.00	0.4
C3	0.50	0.50	1.00	0.2
CR		0		

Notes: thermal conductivity (C1), specific heat capacity (C2), average ground temperature (C3). *CR* is the consistency ratio of the judgment matrix.

Table A3. B2-C Judgment matrix and weight.

B2	C4	C5	C6	C7	ω_i
C4	1.00	1.00	0.33	0.33	0.124
C5	1	1.00	0.33	0.33	0.124
C6	3.00	3.00	1.00	2.00	0.441
C7	3.00	3.00	0.50	1.00	0.312
CR			0.022 < 0.1		

Notes: hydraulic conductivity of phreatic aquifer (C4), hydraulic conductivity of confined aquifer (C5), buried depth of the water table (C6), and thickness of the aquifer (C7). *CR* is the consistency ratio of the judgment matrix.

Table A4. B3-C Judgment matrix and weight.

B3	C8	C9	ω_i
C8	1	2	0.667
C9	0.5	1	0.333
CR		0	

Notes: geomorphology (C8) and thickness ratio of sand/clay (C9). *CR* is the consistency ratio of the judgment matrix.

Table A5. Total ranking and combination weight.

	B1	B2	B3	Combination Weight
	0.540	0.297	0.163	
C1	0.4			0.216
C2	0.4			0.216
C3	0.2			0.108
C4		0.124		0.037
C5		0.124		0.037
C6		0.441		0.131
C7		0.312		0.093
C8			0.667	0.109
C9			0.333	0.054
CR^L		0.010 < 0.1		

Notes: CR^L is the consistency ratio of the total rank.

References

1. Adebayo, T.S. Environmental consequences of fossil fuel in Spain amidst renewable energy consumption: A new insights from the wavelet-based Granger causality approach. *Int. J. Sustain. Dev. World Ecol.* **2022**, *29*, 579–592. [CrossRef]
2. Karmaker, A.K.; Rahman, M.M.; Hossain, M.A.; Ahmed, M.R. Exploration and corrective measures of greenhouse gas emission from fossil fuel power stations for Bangladesh. *J. Clean. Prod.* **2020**, *244*, 118645. [CrossRef]
3. Lamb, W.F.; Wiedmann, T.; Pongratz, J.; Andrew, R.; Crippa, M.; Olivier, J.G.; Wiedenhofer, D.; Mattioli, G.; Al Khourdajie, A.; House, J. A review of trends and drivers of greenhouse gas emissions by sector from 1990 to 2018. *Environ. Res. Lett.* **2021**, *16*, 073005. [CrossRef]
4. Zheng, X.; Streimikiene, D.; Balezentis, T.; Mardani, A.; Cavallaro, F.; Liao, H. A review of greenhouse gas emission profiles, dynamics, and climate change mitigation efforts across the key climate change players. *J. Clean. Prod.* **2019**, *234*, 1113–1133. [CrossRef]

5. Nieto, J.; Carpintero, Ó.; Lobejón, L.F.; Miguel, L.J. An ecological macroeconomics model: The energy transition in the EU. *Energy Policy* **2020**, *145*, 111726. [CrossRef]
6. Langevin, J.; Harris, C.B.; Reyna, J.L. Assessing the potential to reduce US building CO_2 emissions 80% by 2050. *Joule* **2019**, *3*, 2403–2424. [CrossRef]
7. Fragkos, P.; Laura van Soest, H.; Schaeffer, R.; Reedman, L.; Köberle, A.C.; Macaluso, N.; Evangelopoulou, S.; De Vita, A.; Sha, F.; Qimin, C.; et al. Energy system transitions and low-carbon pathways in Australia, Brazil, Canada, China, EU-28, India, Indonesia, Japan, Republic of Korea, Russia and the United States. *Energy* **2021**, *216*, 119385. [CrossRef]
8. Chen, M.; Ma, M.; Lin, Y.; Ma, Z.; Li, K. Carbon Kuznets curve in China's building operations: Retrospective and prospective trajectories. *Sci. Total Environ.* **2022**, *803*, 150104. [CrossRef] [PubMed]
9. Ang, T.-Z.; Salem, M.; Kamarol, M.; Das, H.S.; Nazari, M.A.; Prabaharan, N. A comprehensive study of renewable energy sources: Classifications, challenges and suggestions. *Energy Strategy Rev.* **2022**, *43*, 100939. [CrossRef]
10. Omri, E.; Chtourou, N.; Bazin, D. Technological, economic, institutional, and psychosocial aspects of the transition to renewable energies: A critical literature review of a multidimensional process. *Renew. Energy Focus* **2022**, *43*, 37–49. [CrossRef]
11. Meraj, S.T.; Yu, S.S.; Rahman, M.S.; Hasan, K.; Hossain Lipu, M.S.; Trinh, H. Energy management schemes, challenges and impacts of emerging inverter technology for renewable energy integration towards grid decarbonization. *J. Clean. Prod.* **2023**, *405*, 137002. [CrossRef]
12. Walch, A.; Li, X.; Chambers, J.; Mohajeri, N.; Yilmaz, S.; Patel, M.; Scartezzini, J.-L. Shallow geothermal energy potential for heating and cooling of buildings with regeneration under climate change scenarios. *Energy* **2022**, *244*, 123086. [CrossRef]
13. Romanov, D.; Leiss, B. Geothermal energy at different depths for district heating and cooling of existing and future building stock. *Renew. Sustain. Energy Rev.* **2022**, *167*, 112727. [CrossRef]
14. Caliskan, H.; Açıkkalp, E.; Rostamnejad Takleh, H.; Zare, V. Advanced, extended and combined extended-advanced exergy analyses of a novel geothermal powered combined cooling, heating and power (CCHP) system. *Renew. Energy* **2023**, *206*, 125–134. [CrossRef]
15. Mao, R.; Zhao, Z.; Tian, L.; Fang, T.; Wang, X. Generation of gridded temperature map of constant-temperature layer based on meteorological data for shallow geothermal applications. *Geothermics* **2023**, *113*, 102770. [CrossRef]
16. Yang, H.; Cui, P.; Fang, Z. Vertical-borehole ground-coupled heat pumps: A review of models and systems. *Appl. Energy* **2010**, *87*, 16–27. [CrossRef]
17. Han, Z.; Ran, W.; Tong, H.; Liu, Z. Exploration and evaluation of shallow geothermal energy. *Geol. China* **2007**, *34*, 1115–1121.
18. Zhang, L.; Chen, S.; Zhang, C. Geothermal power generation in China: Status and prospects. *Energy Sci. Eng.* **2019**, *7*, 1428–1450. [CrossRef]
19. Eidesgaard, Ó.R.; Schovsbo, N.H.; Boldreel, L.O.; Ólavsdóttir, J. Shallow geothermal energy system in fractured basalt: A case study from Kollafjørður, Faroe Islands, NE-Atlantic Ocean. *Geothermics* **2019**, *82*, 296–314. [CrossRef]
20. Chiasson, A.D. *Geothermal Heat Pump and Heat Engine Systems: Theory and Practice*; John Wiley & Sons: Hoboken, NJ, USA, 2016.
21. Luo, J.; Luo, Z.; Xie, J.; Xia, D.; Huang, W.; Shao, H.; Xiang, W.; Rohn, J. Investigation of shallow geothermal potentials for different types of ground source heat pump systems (GSHP) of Wuhan city in China. *Renew. Energy* **2018**, *118*, 230–244. [CrossRef]
22. Xu, Y.-S.; Wang, X.-W.; Shen, S.-L.; Zhou, A. Distribution characteristics and utilization of shallow geothermal energy in China. *Energy Build.* **2020**, *229*, 110479. [CrossRef]
23. Li, Z.; Luo, Z.; Wang, Y.; Fan, G.; Zhang, J. Suitability evaluation system for the shallow geothermal energy implementation in region by Entropy Weight Method and TOPSIS method. *Renew. Energy* **2022**, *184*, 564–576. [CrossRef]
24. Hu, Z.; Gao, Z.; Xu, X.; Fang, S.; Zhou, L.; Ji, D.; Li, F.; Feng, J.; Wang, M. Suitability zoning of buried pipe ground source heat pump and shallow geothermal resource evaluation of Linqu County, Shandong Province, China. *Renew. Energy* **2022**, *198*, 1430–1439. [CrossRef]
25. Majorowicz, J.; Grasby, S.E.; Skinner, W.R. Estimation of shallow geothermal energy resource in Canada: Heat gain and heat sink. *Nat. Resour. Res.* **2009**, *18*, 95–108. [CrossRef]
26. Majorowicz, J.A.; Grasby, S.E. Heat transition for major communities supported by geothermal energy development of the Alberta Basin, Canada. *Geothermics* **2020**, *88*, 101883. [CrossRef]
27. Galgaro, A.; Di Sipio, E.; Teza, G.; Destro, E.; De Carli, M.; Chiesa, S.; Zarrella, A.; Emmi, G.; Manzella, A. Empirical modeling of maps of geo-exchange potential for shallow geothermal energy at regional scale. *Geothermics* **2015**, *57*, 173–184. [CrossRef]
28. Blázquez, C.S.; Maté-González, M.Á.; Nieto, I.M.; Martín, A.F.; Gonzalez-Aguilera, D. Assessment of the geothermal potential in the region of Ávila (Spain): An integrated and interactive thermal approach. *Geothermics* **2022**, *98*, 102294. [CrossRef]
29. Meng, B.; Vienken, T.; Kolditz, O.; Shao, H. Evaluating the thermal impacts and sustainability of intensive shallow geothermal utilization on a neighborhood scale: Lessons learned from a case study. *Energy Convers. Manag.* **2019**, *199*, 111913. [CrossRef]
30. Blázquez, C.S.; Nieto, I.M.; Maté González, M.Á.; García, P.C.; Martín, A.F.; González-Aguilera, D. Geophysical exploration for shallow geothermal applications: A case study in Artà, (Balearic Islands, Spain). *Geothermics* **2022**, *105*, 102517. [CrossRef]
31. Luo, J.; Rohn, J.; Xiang, W.; Bertermann, D.; Blum, P. A review of ground investigations for ground source heat pump (GSHP) systems. *Energy Build.* **2016**, *117*, 160–175. [CrossRef]
32. Sarbu, I.; Sebarchievici, C. General review of ground-source heat pump systems for heating and cooling of buildings. *Energy Build.* **2014**, *70*, 441–454. [CrossRef]

33. Karytsas, S.; Theodoropoulou, H. Public awareness and willingness to adopt ground source heat pumps for domestic heating and cooling. *Renew. Sustain. Energy Rev.* **2014**, *34*, 49–57. [CrossRef]
34. Bose, J.E.; Smith, M.D.; Spitler, J.D. *Advances in Ground Source Heat Pump Systems—An International Overview*; China Architecture & Building Press: Beijing, China, 2002; pp. 313–324.
35. Focaccia, S.; Tinti, F.; Monti, F.; Amidei, S.; Bruno, R. Shallow geothermal energy for industrial applications: A case study. *Sustain. Energy Technol. Assess.* **2016**, *16*, 93–105. [CrossRef]
36. Florides, G.; Kalogirou, S. Ground heat exchangers—A review of systems, models and applications. *Renew. Energy* **2007**, *32*, 2461–2478. [CrossRef]
37. Omer, A.M. Ground-source heat pumps systems and applications. *Renew. Sustain. Energy Rev.* **2008**, *12*, 344–371. [CrossRef]
38. Halilovic, S.; Böttcher, F.; Kramer, S.C.; Piggott, M.D.; Zosseder, K.; Hamacher, T. Well layout optimization for groundwater heat pump systems using the adjoint approach. *Energy Convers. Manag.* **2022**, *268*, 116033. [CrossRef]
39. Bernier, M.A. Closed-loop ground-coupled heat pump systems. *Ashrae J.* **2006**, *48*, 12–25.
40. Tang, F.; Nowamooz, H. Factors influencing the performance of shallow Borehole Heat Exchanger. *Energy Convers. Manag.* **2019**, *181*, 571–583. [CrossRef]
41. Chandio, I.A.; Matori, A.N.B.; WanYusof, K.B.; Talpur, M.A.H.; Balogun, A.-L.; Lawal, D.U. GIS-based analytic hierarchy process as a multicriteria decision analysis instrument: A review. *Arab. J. Geosci.* **2013**, *6*, 3059–3066. [CrossRef]
42. Casasso, A.; Sethi, R.G. POT: A quantitative method for the assessment and mapping of the shallow geothermal potential. *Energy* **2016**, *106*, 765–773. [CrossRef]
43. Casasso, A.; Sethi, R. Assessment and mapping of the shallow geothermal potential in the province of Cuneo (Piedmont, NW Italy). *Renew. Energy* **2017**, *102*, 306–315. [CrossRef]
44. Amrani, S.-E.; Merrouni, A.A.; Touili, S.; Dekhissi, H. A multi-scenario site suitability analysis to assess the installation of large scale photovoltaic-hydrogen production units. Case study: Eastern Morocco. *Energy Convers. Manag.* **2023**, *295*, 117615. [CrossRef]
45. Zhang, H.; Li, W.; Miao, P.; Sun, B.; Kong, F. Risk grade assessment of sudden water pollution based on analytic hierarchy process and fuzzy comprehensive evaluation. *Environ. Sci. Pollut. Res.* **2020**, *27*, 469–481. [CrossRef] [PubMed]
46. Xu, S.; Xu, D.; Liu, L. Construction of regional informatization ecological environment based on the entropy weight modified AHP hierarchy model. *Sustain. Comput. Inform. Syst.* **2019**, *22*, 26–31. [CrossRef]
47. Pautz, C.; Santos, A.R.d.; Ferrari, J.L.; Guerra Filho, P.A.; Kunz, S.H.; Dias, H.M.; Moreira, T.R.; Carvalho, R.d.C.F.; Mardeni, V.D.N.; Santos, E.C.d. Mapping the Environmental Vulnerability of a Lagoon Using Fuzzy Logic and the AHP Method. *Water* **2023**, *15*, 2102. [CrossRef]
48. Jovanović, B.; Filipović, J.; Bakić, V. Prioritization of manufacturing sectors in Serbia for energy management improvement–AHP method. *Energy Convers. Manag.* **2015**, *98*, 225–235. [CrossRef]
49. Xie, X.; Yi, Y.; Zhang, H.; Jiang, Y. Theoretical model of absorption heat pump from ideal solution to real solution: Temperature lift factor model. *Energy Convers. Manag.* **2022**, *271*, 116328. [CrossRef]
50. Cherkose, B.A.; Issa, S.; Saibi, H.; ElHaj, K. Building a geospatial model to identify potential geothermal sites in Ayrobera: Afar depression, NE Ethiopia. *Geothermics* **2023**, *110*, 102689. [CrossRef]
51. Dong, J.; He, P.; Liu, H.; Guan, Y.; Liu, H.; Xia, W.; Dong, J. AHP-Based Evaluation of the Suitability of Shallow Geothermal Energy Utilization in GSHP System. *Front. Energy Res.* **2022**, *10*, 183. [CrossRef]
52. Hou, J.; Luo, X.; Zhang, L. Establishment of Evaluation Model for Shallow Geothermal Energy Resource Development Potential Based on Characteristic of Geotemperature. *Earth Sci. Res. J.* **2020**, *24*, 317–325. [CrossRef]
53. Elbarbary, S.; Abdel Zaher, M.; Saibi, H.; Fowler, A.-R.; Saibi, K. Geothermal renewable energy prospects of the African continent using GIS. *Geotherm. Energy* **2022**, *10*, 8. [CrossRef]
54. Li, P.; He, S.; He, X.; Tian, R. Seasonal hydrochemical characterization and groundwater quality delineation based on matter element extension analysis in a paper wastewater irrigation area, northwest China. *Expo. Health* **2018**, *10*, 241–258. [CrossRef]
55. Qian, H.; Li, P. Hydrochemical characteristics of groundwater in Yinchuan plain and their control factors. *Asian J. Chem.* **2011**, *23*, 2927.
56. Yang, C. Research on Comprehensive Evaluation of Shallow Geothermal Energy Resources in Yinchuan Area. Ph.D. Thesis, Chang'an University, Xi'an, China, 2017.
57. *Ningxia Statistical Yearbook*; China Statistics Press: Beijing, China, 2022.
58. Zhang, Y.T.; Hou, K.; Qian, H.; Gao, Y.Y.; Fang, Y.; Tang, S.Q.; Xiao, S.; Ren, W.H.; Qu, W.G.; Zhang, Q.Y. Natural-human driving factors of groundwater salinization in a long-term irrigation area. *Environ. Res.* **2023**, *220*, 115178. [CrossRef] [PubMed]
59. Chen, J.; Qian, H.; Gao, Y.Y.; Li, X.Y. Human Health Risk Assessment of Contaminants in Drinking Water Based on Triangular Fuzzy Numbers Approach in Yinchuan City, Northwest China. *Expo. Health* **2018**, *10*, 155–166. [CrossRef]
60. Chen, J.; Qian, H.; Wu, H. Nitrogen contamination in groundwater in an agricultural region along the New Silk Road, northwest China: Distribution and factors controlling its fate. *Environ. Sci. Pollut. Res.* **2017**, *24*, 13154–13167. [CrossRef]
61. Qian, H.; Li, P.; Howard, K.W.F.; Yang, C.; Zhang, X. Assessment of groundwater vulnerability in the Yinchuan Plain, Northwest China using OREADIC. *Environ. Monit. Assess.* **2012**, *184*, 3613–3628. [CrossRef]
62. Qian, H.; Chen, J.; Howard, K.W.F. Assessing groundwater pollution and potential remediation processes in a multi-layer aquifer system. *Environ. Pollut.* **2020**, *263*, 114669. [CrossRef] [PubMed]

63. Qian, H.; Li, P.; Wu, J.; Zhou, Y. Isotopic characteristics of precipitation, surface and ground waters in the Yinchuan plain, Northwest China. *Environ. Earth Sci.* **2013**, *70*, 57–70. [CrossRef]
64. Zhang, Y.T.; Hou, K.; Qian, H.; Gao, Y.Y.; Fang, Y.; Xiao, S.; Tang, S.Q.; Zhang, Q.Y.; Qu, W.A.; Ren, W.H. Characterization of soil salinization and its driving factors in a typical irrigation area of Northwest China. *Sci. Total Environ.* **2022**, *837*, 155808. [CrossRef]
65. Zhang, G. Is spring the shortest season? *China Meteorological News*, 24 April 2020; p. 4.
66. Chen, J.; Wu, H.; Qian, H.; Li, X.Y. Challenges and prospects of sustainable groundwater management in an agricultural plain along the Silk Road Economic Belt, north-west China. *Int. J. Water Resour. Dev.* **2018**, *34*, 354–368. [CrossRef]
67. Qian, H.; Wu, J.; Zhou, Y.; Li, P. Stable oxygen and hydrogen isotopes as indicators of lake water recharge and evaporation in the lakes of the Yinchuan Plain. *Hydrol. Process.* **2014**, *28*, 3554–3562. [CrossRef]
68. Carslaw, H.S.; Jaeger, J.C.; Feshbach, H. Conduction of heat in solids. *Phys. Today* **1962**, *15*, 74–76. [CrossRef]
69. Esen, H.; Inalli, M. In-situ thermal response test for ground source heat pump system in Elazığ, Turkey. *Energy Build.* **2009**, *41*, 395–401. [CrossRef]
70. Gehlin, S. Thermal Response Test: Method Development and Evaluation. Ph.D. Thesis, Luleå Tekniska Universitet, Luleå, Sweden, 2002.
71. Popov, Y.; Tertychnyi, V.; Romushkevich, R.; Korobkov, D.; Pohl, J. Interrelations between thermal conductivity and other physical properties of rocks: Experimental data. In *Thermo-Hydro-Mechanical Coupling in Fractured Rock*; Birkhäuser: Basel, Switzerland, 2003; pp. 1137–1161.
72. Gustafsson, S.E. Transient plane source techniques for thermal conductivity and thermal diffusivity measurements of solid materials. *Rev. Sci. Instrum.* **1991**, *62*, 797–804. [CrossRef]
73. Boumaza, T.; Redgrove, J. Use of the transient plane source technique for rapid multiple thermal property measurements. *Int. J. Thermophys.* **2003**, *24*, 501–512. [CrossRef]
74. Wu, X.H.; Qian, H.; Yu, D.M.; Zhang, Q.; Yan, Z.; Wang, W.; Ji, Y.D.; Liu, H.M.; Mao, Z.L.; Zhao, Q. *Investigation and Assessment of Rational Allocation of Groundwater Resources in the Yinchuan Plain*; Geology Publish House: Beijing, China, 2008; pp. 171–173.
75. Wang, T. Suitability Evaluation on the Shallow Geothermal Energy in Major Cities Along the Yellow River, Ningxia Section. Master's Thesis, Chang'an University, Xi'an, China, 2011.
76. Saaty, T.L. How to make a decision: The analytic hierarchy process. *Eur. J. Oper. Res.* **1990**, *48*, 9–26. [CrossRef]
77. *DZ/T0225-2009*; Specification for Shallow Geothermal Energy Investigation and Evaluation. Ministry of Land and Resources of the People's Republic of China: Beijing, China, 2009.
78. Wang, G.; Wang, W.; Luo, J.; Zhang, Y. Assessment of three types of shallow geothermal resources and ground-source heat-pump applications in provincial capitals in the Yangtze River Basin, China. *Renew. Sustain. Energy Rev.* **2019**, *111*, 392–421. [CrossRef]
79. Wang, W.; Wang, G.; Liu, C.; Li, J. Research on the comprehensive thermal conductivity of shallow rock and soil in major cities in the North China Plain. *Acta Geol. Sin.* **2020**, *94*, 2089–2095.
80. Bai, X.; Li, Z.; Liu, S.; Song, J. Study on comprehensive thermal conductivity of shallow rock and soil in alluvial plain of the Yellow River(Northwest Shandong)—Taking Linqing City as an example. *Urban Geol.* **2021**, *16*, 66–74.
81. Zhou, Y.; Mu, G.; Liu, J.; Zhang, H.; Zhang, L.; Jing, G. Shallow Geothermal Energy Resources Occurrence Regularity of Typical Geomorphological Units. *Bull. Geol. Sci. Technol.* **2018**, *37*, 232–238+268.
82. Zhang, L.; Zhou, Y.; Liu, J.; Jin, G.; Zhang, Y. Analysis on thermal conductivity of typical geomorphological units in Shaanxi Province based on superposition method. *Geol. Surv. China* **2020**, *7*, 91–96.
83. Schön, J.H. Thermal Properties. In *Developments in Petroleum Science*; Elsevier: Amsterdam, The Netherlands, 2015; Volume 65, pp. 369–414.
84. Zhang, N.; Wang, Z. Review of soil thermal conductivity and predictive models. *Int. J. Therm. Sci.* **2017**, *117*, 172–183. [CrossRef]
85. Ambreen, T.; Kim, M.-H. Influence of particle size on the effective thermal conductivity of nanofluids: A critical review. *Appl. Energy* **2020**, *264*, 114684. [CrossRef]
86. Zhou, Y.; Dai, L.; Tian, Z.; Yu, C.; Zhang, Z.; Liu, W.; PeI, L. Core characteristics and Quaternary stratigraphic division of borehole QK4 in southern Lubei Plain. *Geophys. Geochem. Explor.* **2023**, *47*, 55–64.
87. Li, J.; Zheng, J.; Lei, X.; Du, J.; Li, F.; Jia, z.; Liu, A. Analysis of quaternary thermal properties and influencing factorson shallow geothermal energy exploitation in Beijing plain. *Geol. China* **2022**, *49*, 1543–1554.
88. Ruan, C.; Feng, S.; Mou, S.; Cheng, W.; Zhao, S. Evaluation of Shallow Geothermal Energy Resources and Analysis of Development and Utilization Conditions in Tianjin. *Hydrogeol. Eng. Geol.* **2017**, *44*, 158–163.
89. Zhao, L.; Sun, X.; Zhan, Y.; Han, J.; Yang, H.; Wang, P.; Liu, X. Characteristics of the three-dimensional deep electrical structure in the Helan Mountains-Yinchuan Basin and its geodynamic implications. *Sci. China Earth Sci.* **2023**, *66*, 505–520. [CrossRef]
90. Walch, A.; Mohajeri, N.; Gudmundsson, A.; Scartezzini, J.-L. Quantifying the technical geothermal potential from shallow borehole heat exchangers at regional scale. *Renew. Energy* **2021**, *165*, 369–380. [CrossRef]
91. Wang, W.; Wang, G.; Zhu, X.; Liu, Z. Characteristics and potential of shallow geothermal resources in provincial capital cities of China. *Geol. China* **2017**, *44*, 1062–1073.
92. Shen, J.; Zhou, C.; Luo, Y.; Tian, Z.; Zhang, S.; Fan, J.; Ling, Z. Comprehensive thermal performance analysis and optimization study on U-type deep borehole ground source heat pump systems based on a new analytical model. *Energy* **2023**, *274*, 127367. [CrossRef]

93. Dehkordi, S.E.; Schincariol, R.A. Effect of thermal-hydrogeological and borehole heat exchanger properties on performance and impact of vertical closed-loop geothermal heat pump systems. *Hydrogeol. J.* **2014**, *22*, 189. [CrossRef]
94. *GB/T 2589—2020*; State Administration for Market Regulation of China; General Principles for Calculation of the Comprehensive Energy Consumption. China Standard Press: Beijing, China, 2020.
95. *DZT 0331-2020*; Estimation and Evaluation Method of Geothermal Resources. Ministry of Natural Resources of the People's Republic of China: Beijing, China, 2020.
96. Feng, B.; Ma, Y.; Qi, Y.; Zhong, Y.; Sha, X. Health risk assessment of groundwater nitrogen pollution in Yinchuan plain. *J. Contam. Hydrol.* **2022**, *249*, 104031. [CrossRef]